2016

# Complex coastal change in response to autogenic basin infilling: An example from a sub-tropical Holocene strandplain

Christopher J. Hein
*Virginia Institute of Marine Science*

DM FitzGerald

LHP de Souza

IY Georgiou

IV Buynevich

*See next page for additional authors*

## Authors

Christopher J. Hein, DM FitzGerald, LHP de Souza, IY Georgiou, IV Buynevich, and Et al.

# Complex coastal change in response to autogenic basin infilling: An example from a sub-tropical Holocene strandplain

CHRISTOPHER J. HEIN*, DUNCAN M. FITZGERALD†, LUIS H. P. DE SOUZA‡, IOANNIS Y. GEORGIOU§, ILYA V. BUYNEVICH¶, ANTONIO H. DA F. KLEIN**, JOÃO THADEU DE MENEZES‡††, WILLIAM J. CLEARY‡‡ and THELMA L. SCOLARO††

*Department of Physical Sciences, Virginia Institute of Marine Science, College of William and Mary, Gloucester Point, VA 23062, USA (E-mail: hein@vims.edu)

†Department of Earth and Environment, Boston University, Boston, MA 02215, USA

‡Laboratory of Geological Oceanography, Laboratory of Biodiversity Informatics and Geomatics, UNIVALI – CTTMAR, Itajaí, SC 88300-000, Brazil

§Department of Earth and Environmental Sciences, The University of New Orleans, New Orleans, LA 70148, USA

¶Department of Earth and Environmental Science, College of Science and Technology, Temple University, Philadelphia, PA 19122, USA

**Laboratory of Coastal Oceanography, Department of Geosciences, Center for Philosophy and Human Sciences, Federal University of Santa Catarina, University Campus – Trindade, Florianópolis, SC 88040-900, Brazil

††Environmental Modeling & Risk Assessment, Acquadinamica Inc., Balneário Camboriú, SC 88330-000, Brazil

‡‡Center for Marine Science, University of North Carolina at Wilmington, Wilmington, NC 28403, USA

**ABSTRACT**

Thick bay-fill sequences that often culminate in strandplain development serve as important sedimentary archives of land–ocean interaction, although distinguishing between internal and external forcings is an ongoing challenge. This study employs sediment cores, ground-penetrating radar surveys, radiocarbon dates, palaeogeographic reconstructions and hydrodynamic modelling to explore the role of autogenic processes – notably a reduction in wave energy in response to coastal embayment infilling – in coastal evolution and shoreline morphodynamics. Following a regional 2 to 4 m highstand at *ca* 5·8 ka, the 75 km$^2$ Tijucas Strandplain in southern Brazil built from fluvial sediments deposited into a semi-enclosed bay. Holocene regressive deposits are underlain by fluvial sands and a Pleistocene transgressive–regressive sequence, and backed by a highstand barrier-island. The strandplain is immediately underlain by 5 to 16 m of seaward-thickening, fluvially derived, Holocene-age, basin-fill mud. Several trends are observed from the landward (oldest) to the seaward (youngest) sections of the strandplain: (i) the upper shoreface and foreshore become finer and thinner and shift from sand-dominated to mud-dominated; (ii) beachface slopes decrease from >11° to *ca* 7°; and (iii) progradation rates increase from 0·4 to 1·8 m yr$^{-1}$. Hydrodynamic modelling demonstrates a correlation between progressive shoaling of Tijucas Bay driven by sea-level fall and sediment infilling and a decrease in onshore wave-energy transport from 18 to 4 kW m$^{-1}$. The combination of allogenic (sediment supply, falling relative sea-level and geology) and autogenic (decrease in wave energy due to bay shoaling) processes drove the development of a regressive system with characteristics that are rare, if not unique, in the Holocene and rock records. These findings demonstrate the

complexities in architecture styles of highstand and regressive systems tracts. Furthermore, this article highlights the diverse internal and external processes and feedbacks responsible for the development of these intricate marginal marine sedimentary systems.

**Keywords** Chenier, coastal progradation, GPR, regression, strandplain, upland migration potential, wave energy.

## INTRODUCTION

At the most fundamental level, centennial to millennial-scale evolution of coastal sedimentary systems are governed by the creation and filling of accommodation, as controlled by the rate or direction of relative sea-level (RSL) change, sediment supply rates and antecedent topography (Curray, 1964; Belknap & Kraft, 1985; Roy *et al.*, 1994). These are, in turn, driven by allogenic processes operating at global to regional scales and, to a lesser extent, autogenic processes acting at local scales. Coastal allogenic processes include: eustacy and glacio-isostacy and hydro-isostacy (Milne *et al.*, 2009); uplift and subsidence caused by basin-wide tectonics; climate-driven and human-driven changes in sediment supply (Leeder *et al.*, 1998; Kirwan *et al.*, 2011; Milliman & Farnsworth, 2011; Hein *et al.*, 2014a); and changes in meteorological or oceanographic conditions such as storminess and wave energy or directionality (Dominguez *et al.*, 1992). Numerous autogenic processes intrinsic to specific depositional or geomorphic environments also play a critical role in coastal evolution, primarily in the reworking of sediments to fill accommodation with varying volumes and hypsometry. These processes can include sediment production *in situ* or proximal to the coastal depocentre (i.e. in carbonate environments) (e.g. Wright & Burchette, 1996); river downcutting or avulsions (e.g. Muto & Steel, 2004; Jerolmack & Paola, 2010); interactions between local wave climates and shoreline progradation (Ashton & Giosan, 2011) or *in situ* reef development (Andrade *et al.*, 2003); subsidence caused by fluid extraction (Poland & Davis, 1969; Holzer & Galloway, 2005) or substrate compaction (Meckel *et al.*, 2007; Törnqvist *et al.*, 2008); or local geological and geomorphic controls on accommodation availability during transgression or regression (Simms & Rodriguez, 2015).

Much of the scientific discourse regarding the impacts of climate change on coastal systems, and the ecological and human communities they support, focuses on projected changes in allogenic processes: accelerations in the rate of RSL rise (Church *et al.*, 2014); enhanced frequency and intensity of storms (Elsner *et al.*, 2008; Lin *et al.*, 2012); and human-induced changes in sedimentation (Blum & Roberts, 2009; Anderson *et al.*, 2010). Comparatively little attention has been given to autogenic processes which, although they act on much smaller scales, have the potential to impart outsized stratigraphic signatures coastal systems as they develop in response to environmental change.

Strandplains are broad accumulations of sediment formed in parallel or semi-parallel ridges oriented approximately parallel to the coastline (Roy *et al.*, 1994), and are typically characterized by long-term, continuous progradation. Individual beach ridges (clastic sand and/or gravel, often with shell fragments, formed by constructional wave activity above the normal high spring tide level; Otvos, 2000; Hesp *et al.*, 2005) or foredune ridges (vegetated dunes formed on the backshore of beaches by aeolian sand deposition; Hesp *et al.*, 2005) are added to the strandplain as a function of sediment supply, RSL trends and storm climate (Roy *et al.*, 1994; Otvos, 2005; Tamura, 2012). Sediments are preserved through the 'stranding' of depositional sequences as successive ridges are added along the seaward side of the plain. In this manner, an individual strandplain can act as a several-kilometre-long sediment core, laid on its side and preserved in an easily-accessible terrestrial environment. This allows the foredune or beach ridges comprising these systems to potentially serve as continuous recorders of Holocene environmental change (Schaeffer *et al.*, 2012). Studies of such strandplain sequences in southern Brazil have identified subtle changes in the rate and/or direction of RSL change (Hein *et al.*, 2013), storm events (Buynevich *et al.*, 2007), and changes in local wave and wind regimes (Dominguez *et al.*, 1987, 1992; Andrade *et al.*, 2003; Sawakuchi *et al.*, 2008).

The present study employs records provided within the Tijucas Strandplain in southern Brazil (Fig. 1) to explore the role of autogenic changes in wave energy, driven by allogenic RSL change and sediment delivery, and the attendant implications of this feedback for coastal evolution. New geophysical, morphological, sedimentological and chronological data are presented, and combined with process-based analyses (hydrodynamic modelling), to provide insight into the shoreline processes acting across multiple transgressive/regressive cycles responsible for filling Tijucas Bay and produce the complex morphologies observed in the modern strandplain and beach. This approach enables investigation of the role of bay infilling in coastal evolution and shoreline morphodynamics, and exploration of sediment-supply driven autogenic processes governing coastal response to RSL change.

## BACKGROUND: TIJUCAS STRANDPLAIN, SOUTHERN BRAZIL

### Holocene sea-level history

Following the last glaciation, relative sea-level (RSL) in much of the Southern Hemisphere reached modern levels at 6·9 to 7·7 ka and continued to rise to a highstand elevation of 1 to 4 m above modern mean sea-level (m MSL) at 5·5 to 6·0 ka (Isla, 1989; Mitrovica & Milne, 2002; Milne *et al.*, 2005; Angulo *et al.*, 2006). This complex history results from global hydro-isostasy: collapsing forebulges in previously glaciated continental margins during the mid-Holocene created accommodation in those previously glaciated regions, causing a syphoning of water from far-field (generally southern ocean) regions (Mitrovica & Milne, 2002). Additional accommodation in the near field (previously glaciated margins) was created by hydro-isostatic loading of the continental margin, thus producing additional syphoning and accounting for an additional 40% of sea-level fall in far-field regions (Milne *et al.*, 2005).

Although no reliable sea-level data have been reported for the Santa Catarina coast prior to *ca* 6·5 ka, rheological models predict that sea-level in this region reached modern elevations at *ca* 7·6 ka, followed by a highstand lasting as long as 2000 years (Fig. 2). RSL has since fallen relatively smoothly (rate: *ca* 0·6 m/1000 years), or with gentle oscillations, to modern elevations (Angulo *et al.*, 2006).

## Coastal geological setting

Falling RSL in southern Brazil during the middle to late Holocene, coupled with an abundant supply of sediment, has resulted in a mixed, forced/normal regression and the production of extensive strandplains, partially smoothing the irregular, headland-dominated coast. At Tijucas (Santa Catarina, Brazil) these processes formed an eastward-facing strandplain that is *ca* 5 km wide and extends 12 km along the coast (Fig. 1).

The Tijucas Strandplain is composed of sediments derived almost singularly from the Tijucas River (Schettini *et al.*, 2010) which flows through the middle of the northern sector of the plain (Figs 1 and 3). A small (drainage basin area: 150 km$^2$) local river, the Inferninho, drains into the southern sector of Tijucas (Fig. 1B). The Tijucas River is a moderate-sized drainage system, with a catchment of 2420 km$^2$ and an average discharge of 40 m$^3$ sec$^{-1}$ (Agencia Nacional da Água, 2000). Upstream, the drainage becomes segmented and narrower, and is bounded by increasingly higher topography. The local geology results from the presence of a series of coast-parallel grabens and horsts that were created by the Tertiary collapse of a large Cretaceous plateau (Zalán & Oliveira, 2005), that created rocky scarps along an elongated east–west trending high that separates the Pelotas and Santos marginal basins (Giannini, 1993; Caruso *et al.*, 2000).

The geology of the Tijucas drainage basin is dominated by Neoproterozoic granites, and metavolcanosedimentary (Rio do Oliveira Formation) and metasedimentary (Botuverá Formation) rocks of the Brusque fold belt, as well as arc-related Proterozoic granites and granodiorites of the Florianópolis batholith (Basei *et al.*, 2011; Caruso, 2004; Jacques *et al.*, 2014). Intense weathering of this bedrock has produced a saprolite that is tens of metres thick. Erosion of the saprolite during high precipitation events supplies large quantities of fine-grained sediment as well as sand and fine gravel to the Tijucas coast; the Tijucas River turns chocolate brown and is thick with suspended sediment (FitzGerald *et al.*, 2007). Although average suspended-sediment concentrations in the Tijucas River have been measured to be 70 mg L$^{-1}$ (Schettini *et al.*, 1996), the high relief of the Tijucas drainage basin yields flood flows that have been observed to increase average discharges by an estimated two orders of magnitude during periods of intense rainfall. Sediments exported from the Tijucas River are dispersed along the shore-

**Fig. 1.** (A) Map of the coast of Santa Catarina, Brazil. Yellow line: landward boundary of Quaternary deposits (after Horn Filho & Diehl, 1994). (B) Digital elevation model of Tijucas Strandplain and Tijucas Bay, derived from topographic and bathymetric databases available from the Santa Catarina state government (SDS, 2013). The Holocene highstand shoreline (yellow line) is mapped from the landward extent of strandlines visible in 2014 satellite imagery (Google Earth), supplemented with ground-penetrating radar data, sediment cores, radiocarbon dates and topographic data: mMSL, metres above modern mean sea-level, in WGS 84 datum. (C) Tijucas Beach during calm conditions in March 2009, four months following a large flood event on the Tijucas River (photograph credit: C. Hein). (D) Image of Tijucas Beach during a moderate-energy event in November 2012 (photograph credit: L. de Souza). The lower beach face was coated with *ca* 2 cm of fine silt and clay during this event.
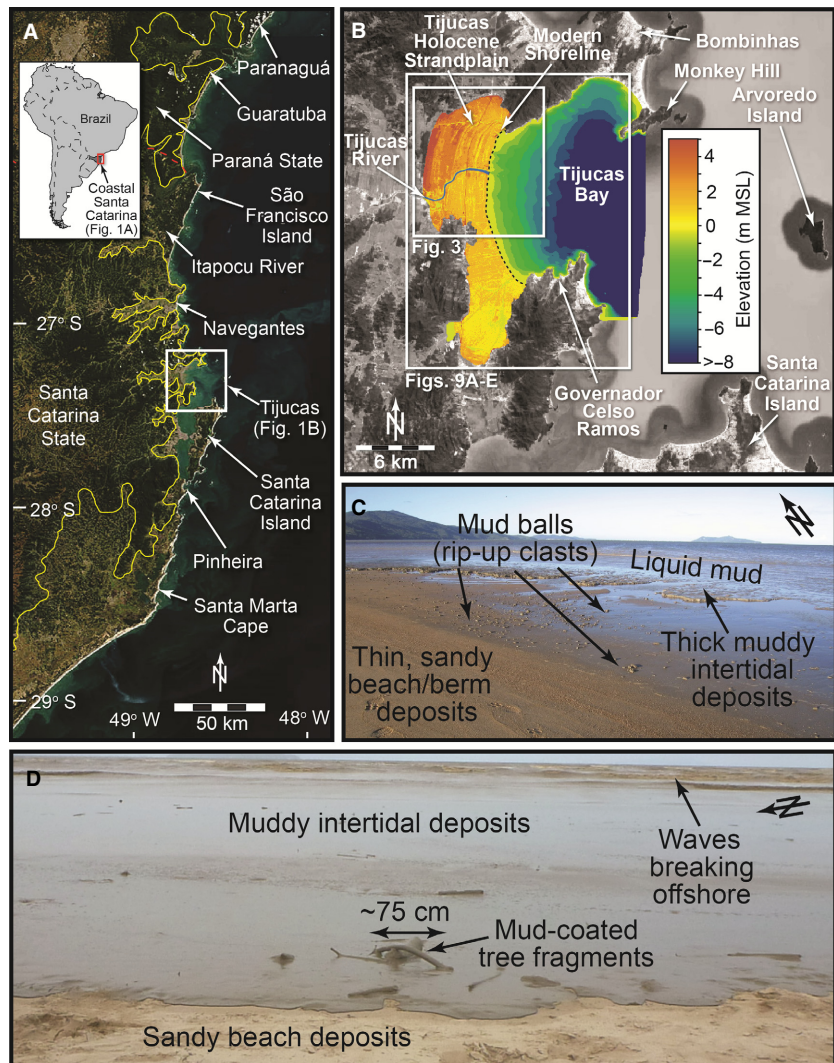
line, resulting, through time, in the formation of concentric semi-circular shorelines co-deposited with strandplain progradation (Figs 1 and 3).

Tijucas is fronted by a semi-enclosed, 100 km$^2$ embayment protected from coastal ocean processes by the presence of high-relief (maximum elevation: >200 m) bedrock headlands and islands. The bay deepens gently in the offshore direction, reaching a maximum depth of 15 m near its opening to the coastal ocean (Fig. 1B). These headlands extend 10 to 18 km seaward of the strandplain shoreline; they probably were islands during the mid-Holocene highstand, similar to a series of isolated bedrock islands located as far as 25 km offshore of the modern shoreline (for example, Arvoredo Island, Fig. 1B). Today, these headlands are connected to the mainland by alluvial and littoral deposits.

The climate at Tijucas is subtropical, with average precipitation (1415 mm yr$^{-1}$) approximately

evenly distributed throughout the year. Prevailing winds are from the north-east, but the wind regime is dominated by the passage of moderately-strong cold fronts that induce southerly winds (Klein, 1997) and occasional cyclones (Barletta & Calliari, 2001). Intense storms are rare. Modern weather patterns are dominated by two high pressure masses: the Polar Migratory Anticyclone (PMA) which is responsible for small, frequent winter storms and southerly winds (Orselli, 1986); and the South Atlantic Tropical Anticyclone (SATA), which controls prevailing north-east winds. During the austral winter, the PMA dominates and moisture to the Tijucas Basin is derived from the nearby South Atlantic Ocean. During the austral summer, the SATA dominates and moisture is delivered from the tropical south Atlantic, over the Amazon Basin, by the South America Summer Monsoon (SASM; Zhou & Lau, 1998; Marengo *et al.*, 2012).
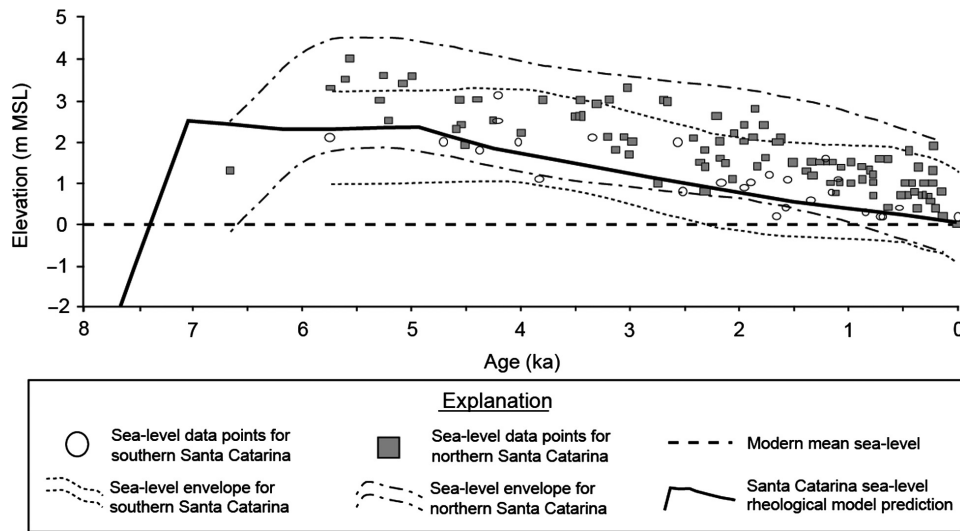
**Fig. 2.** Relative sea-level curves for southern Brazil based on glacio-hydroisostatic model predictions (Milne *et al.*, 2005) and sea-level indicator data from radiocarbon analyses of encrusting gastropods [vermetid: *Petaloconchus* (Macrophragma) varians] (Angulo *et al.*, 2006). Index points have an assumed vertical error of ±1 m (Angulo *et al.*, 1999): m MSL, metres above modern mean sea-level.

The mean tidal range at Tijucas is 0·8 m (spring range: 1·2 m) (Truccolo, 1998). Deepwater wave heights are 1·0 to 1·5 m and sea swells are bimodal: a 12 sec swell from the south has significant heights of 1·25 to 2·00 m, and an 8 sec swell from the east has an average significant height of *ca* 1·25 m (Araújo *et al.*, 2003). The larger southerly swell results in net northerly longshore transport along the Santa Catarina coast (Giannini, 1993). However, transport rates and directions are highly variable due to local wave refraction/diffraction around bedrock headlands (FitzGerald *et al.*, 2007; Siegle & Asp, 2007). The high degree of coastal indentation and gentle, even slope of Tijucas Bay cause ocean swells to be nearly fully refracted; waves breaking along the swash-aligned Tijucas shore are commonly <0·5 m. Suspended-sediment concentrations along the shoreline and throughout the bay are generally very high (several grams per litre): density profiles and sediment cores collected at different times during the year and in different years throughout the bay have documented a 10 to 70 cm thick fluid mud layer resting on top of a con-solidated muddy bed (Schettini *et al.*, 2010).

## METHODS

The middle to late-Holocene regressive bay infilling sequence at Tijucas was investigated using a variety of field (Fig. 3) and laboratory-based approaches, including morphological, sed-imentological (Figs 4 to 6), geophysical (Figs 5 to 7), geochronological (Fig. 8; Table 1) and pro-cess-based (Figs 9 and 10) techniques.

## Field and laboratory data collection

Thirty kilometres of ground-penetrating radar (GPR) profiles were collected along predomi-nantly shore-normal transects throughout the Tijucas Strandplain (Fig. 3). These data were collected using a digital Geophysical Survey Systems Inc. (GSSI, North Salem, NH, USA) SIR-2000 system with a 200 MHz monostatic antenna with a two-way travel-time (TWTT) range of 150 to 300 nsec. The output from this system penetrated to 4 to 8 m depth; penetration was commonly limited by signal attenuation in fine-grained sediment. Ground-penetrating radar data were post-processed (site-specific data fil-tering, variable-velocity migration, gain control) and time-depth converted (based on hyperbola fitting and depth to reflector ground-truthing) using the RadExplorer (DECO-Geophysical Co. Ltd., Moscow, Russia) software package. Profiles were topographically corrected using RTK-GPS elevation data points collected along the profile lines at 5 m intervals.

More than 50 km of topographic data were collected using a Trimble R6 global-positioning system (Trimble Navigation Limited, Sunnyvale, CA, USA) with a real-time kinematics (RTK-GPS) system (Datum: SAD69). Data were col-
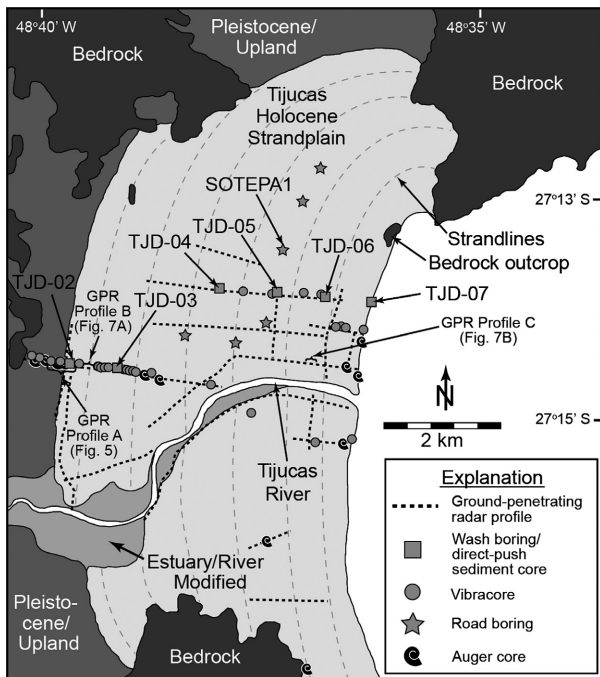
**Fig. 3.** Simplified geomorphological map of Tijucas (map extent shown in Fig. 1), based on GIS and ground mapping. Locations of GPR profile lines, wash boring/direct-push cores, vibracores and auger cores are shown.

lected at between 1 m and 15 m point spacing. Closer spaced data were collected along GPR profiles for use in topographic corrections. The topographic data supplement existing topographic and bathymetric databases available from the Santa Catarina state government [Secretaria de Estado do Desenvolvimento Sustentável (SDS), 2013]. All horizontal and vertical data presented here are given in the WGS84 datum.

As part of a comprehensive study of the Tijucas Strandplain, a suite of 2 to 4 m deep hand-auger cores (23 total), 4 to 6 m deep vibracores (51 total) and six 17 to 26 m deep wash borings were collected across the study area. Wash-bore cores used a combination of fluid wash and percussion direct push that provided for 45 cm of continuous recovery every metre. Sediment coring was focused along two semi-parallel, shore-normal transects, starting landward of the mid-Holocene highstand deposits identified by FitzGerald *et al.* (2007) and extending to the modern intertidal zone (Fig. 3). Shallow cores were used primarily to ground-truth interpretations of lithological units in GPR profiles; most are too shallow to provide information on the deep basin-infilling sequences and are thus not included in this study. Deep cores

provided information on the overall basin-infilling sequence at Tijucas. These were supplemented with basic lithological data from 51 road borings provided by local road drilling/construction companies [Sotepa, Ltda (Florianópolis, SC, Brazil); and SOLO Sondagem e Construções Ltda (Balneário Camboriú, SC, Brazil)]. Due to inconsistent and incomplete reporting of lithologies, including the reporting of markedly different sediment characteristics in cores collected only metres apart, only those few select core logs with the most detailed and consistent records are incorporated into analyses and presented here. Deep sediment core data were spatially analysed and interpreted in three-dimensional (3D) GIS framework using both ArcGIS (Environmental Systems Research Institute, Inc., Redlands, CA, USA) and Rockworks (RockWare, Inc., Golden, CO, USA) software packages.

Vibracores were opened, logged, photographed and sampled at the Laboratory for Geological Oceanography at the Universidade do Vale do Itajaí (UNIVALI). Auger cores and continuous (percussion direct-push) sections of wash borings were described and photographed in the field. At least one sample was collected within each sedimentological unit (2 to 20 cm sampling intervals). Selected sediment samples were prepared and analysed using combined wet/dry sieve [0·5 phi ($\varphi$) intervals] techniques to determine particle-size characteristics (Folk, 1980).

Major lithological boundaries were determined from sediment cores (Figs 4 to 6), GPR-reflection profiles (Figs 5 and 6) and chronological data. The latter were provided by radiocarbon analyses of 30 samples of whole or broken mollusc shells, wood debris or peat matter collected from sediment cores (Table 1). All radiocarbon analyses were performed at the National Ocean Sciences Accelerator Mass Spectrometry Facility (NOSAMS; Woods Hole, MA, USA). Dated terrestrial samples were calibrated using OxCal 4.2 (Bronk Ramsey, 2009) with SHcal13 (Hogg *et al.*, 2013) calibration curves (Table 1). Marine samples (molluscs) were calibrated using IntCal13 (Reimer *et al.*, 2013) with a marine reservoir correction of 8 ± 17 years (Angulo *et al.*, 2005). All dates presented in the text are calibrated, 2-sigma (2-α) years before present (BP; present = 1950).

## Palaeogeographic reconstructions and hydrodynamic modelling

To assess changes in wave climate through time, the Simulating WAves in the Nearshore (SWAN)

model was used; a third-generation wave model (Booij *et al.*, 1999) that computes random, short-crested wind-generated waves in coastal regions and inland waters. The SWAN model can account for many physical processes, including wave propagation in time and space, shoaling, refraction due to current and depth, wave generation by wind, three-wave and four-wave interactions, whitecapping, bottom friction and depth-induced breaking, dissipation due to vegetation and wave-induced set-up.

Models were setup for four time steps using RSL elevations derived from the mid-point of the RSL envelope for northern Santa Catarina (Fig. 2; Angulo *et al.*, 2006): the mid-Holocene highstand (5800 BP; 3·1 m MSL), 2500 BP (2·2 m MSL), 1000 BP (1·4 m MSL) and modern (−60 BP; 0 m MSL). The sea-level envelope mid-point was used to reduce model redundancy, rather than using a range of elevations representing a given time, because the mid-point of the envelope is the only part that crosses modern MSL at present; the mid-point also matches the local sea-level model predictions of Milne *et al.* (2005) closer than either the low or high-end MSL elevations captured by the sea-level envelopes (Fig. 2). Bathymetric grids used in modelling were constructed by gridding (interpolating) reconstructed bathymetric data based on modern bathymetry, modern topography and stratigraphic data. Grids were extended to 12 km offshore of the modern shoreline, a position beyond the southern headlands and parallel with the northern headland at Tijucas (Fig. 1B). Modern depths at this location are 25 to 30 m. Palaeoshoreline positions (Fig. 9) were determined along a single cross-shore profile (Fig. 4) from core stratigraphic and chronological data and a variable-rate progradation model (Fig. 8A). The latter was computed by substituting 'distance from the modern shoreline' for 'depth in a single core' in the Bayesian age-depth modelling software package Clam 2.1 (Blaauw, 2010). These positions were extrapolated alongshore by mapping of semi-parallel strandlines visible in both high-resolution topographic [digital elevation models (DEMs); SDS, 2013 and new RTK-GPS and dGPS data] and imagery data (Google Earth™ imagery and ArcGIS basemaps). Each shoreline was assigned a single elevation with respect to modern mean sea-level based on the elevation of the modern natural topography at the position of the shoreline along the 2D cross-shore profile (Fig. 4) (5800 BP: +6 m; 2500 BP: +4·5 m; 1000 BP: +3·4 m; Modern: +1·5 m).

Onshore of the modern shoreline, palaeogeographic reconstructions of the 5800 BP, 2500 BP and 1000 BP bathymetric surfaces are based on onshore core-log data supplemented with additional control points positioned along the same palaeo-shoreline positions as the sediment cores (Fig. 9A). Offshore of the modern shoreline, reconstructed bathymetric surfaces are based on modern bathymetric data from *ca* 1000 bathymetric points within the gridding region available from SDS (2013) (Fig. 9A). Based on two observations, it was assumed that the bay filled at equal rates alongshore: (i) individual strandlines (shorelines) can be traced continuously alongshore across the strandplain, indicating longshore reworking and sand and mud within a time period shorter than the progradation of individual shorelines; and (ii) the modern arcuate shoreline is fronted by smooth, shore-parallel depth contours, rather than a fluvial-dominated subaqueous delta, indicating rapid dispersal of fine sediments throughout the embayment. That is, at a given time, any location along a shore-parallel transect in the palaeo-bay would have had the same depth. Thus, the same depth of the bay derived from a single sediment core is assigned to all control points along the same modern strandline (palaeo-shoreline) as that core. Offshore, bathymetric data are modified to reflect the filling of the bay over time. For the 5800 BP surface, a nearshore slope of 0·109° is calculated based on the average slope of the base of the regressive unit in the seaward section of the Tijucas Strandplain (seaward of core TJD3; Fig. 5). The depths of all offshore bathymetric control points (those points seaward of the modern shoreline; Fig. 9A) are increased according to their distance offshore to their assumed depths according to this constant slope. This same approach is taken for the bathymetric points to create the 2500 BP and 1000 BP surfaces, assuming a linearly decreasing (with time) offshore slope between the 5800 BP slope and the slope of the modern bay in the defined gridding area (0·067°) (Table 2). This approach has the implicit assumption that deeper sections of the bay shallowed at a constant rate during the past 5800 years as the bay was filled with sediments from the Tijucas River, with rates dictated by available accommodation. Assuming rapid dispersal of fluvial sediment throughout the bay and a constant sediment supply through time (which cannot be known with available data), then accumulation rates should be the same through time at any location distal to the river; hence, this assumption is the only viable option

for artificially stripping bay sediment to a calculated palaeo-depth required by the difference between highstand and modern offshore slopes.

These input data were gridded at 25 m cell resolution via kriging in Surfer™ using an exponential semi-variogram model with an anisotropy ratio of 2. The results are a set of approximately smoothly seaward-dipping bathymetric surfaces with offshore slopes that gradually shallow through time (Fig. 9).

Model grids were set up with constant resolution in both easting and northing directions of *ca* 100 m in Cartesian coordinates. The model was forced at marine open boundaries with wave observations and model reanalysis results from Araújo *et al.* (2003), and using seasonal mean and maximum wave climate from re-analysis conducted for autumn and spring conditions, and was the same for each time step. Additionally, storm wave conditions were considered based on the same data set (Araújo *et al.*, 2003). Offshore open boundaries are located in depths of 65 to 85 m to ensure insignificant bed interaction with the bed near the boundary. The JONSWAP spectral distribution was used and frequencies were selected spanning all observed conditions from observations, mean wave direction and mean significant wave height and period, utilizing the standard deviation of the wave direction to define the directional spreading using analysis by Araújo *et al.* (2003). All simulations accounted for similar wave transformation across all time steps and included dissipation due to shoaling, bottom friction refraction, diffraction and dissipation due to breaking. While wind growth and hence wind setup was not active, wave setup was included for all simulations.

## RESULTS: HOLOCENE DEPOSITIONAL SEQUENCES AT TIJUCAS

The Tijucas Basin is composed of a series of seaward-dipping sedimentary units with bounding surfaces that are steeper in landward sections (0·5° to 0·6°) and shallow (<0·2°) seaward. These units are interpreted to have been deposited during multiple transgressive/regressive cycles of the late Pleistocene and Holocene.

### Unit I: Basal terrestrial unit

The Holocene sedimentary sequence at Tijucas is underlain by a basal, coarse-grained, oxidized (light tan to orange colour), poorly sorted sedimentary unit typically composed of angular to sub-angular silty coarse sand/granule with some large (*ca* 2 cm diameter) sub-rounded to sub-angular pebbles (Unit I). In most locations, wash boring/direct-push cores were only able to penetrate a maximum of <1 m into this unit (Fig. 4). The upper contact of this unit, located between −11 m and −21 m MSL (deeper in seaward sections), is sharp, and uppermost sediments are moderately to highly oxidized, indicative of surface exposure and erosion.

Given the immaturity and degree of oxidation of the sediments which compose this unit, Unit I is interpreted as fluvial in origin, probably attributable to the meandering Tijucas River at a lower stand of RSL. Based on facies relationships with overlying deposits, Unit I probably predates the marine Oxygen Isotope Stage (OIS) 5e (*ca* 125 ka) RSL highstand. However, no datable material was recovered from this unit. The seaward-most sediment core, TJD07, collected within 50 m of the modern shoreline (Figs 3 and 4), bottomed at an impenetrable layer at only −15 m MSL. Bottom sediments were highly oxidized silt, fine sand and clay. It is unclear if these sediments are from this same fluvial unit or shallow, chemically eroded saprolitic bedrock, similar to the bedrock outcrop found along the modern Tijucas shoreline 900 m north of core TJD07 (Fig. 3).

### Unit II: Pleistocene transgressive/regressive units

The basal fluvial unit is overlain by a 0·5 to 6·0 m thick series of fining-upward and coarsening-upward sequences (Unit II). Basal sections of this unit are composed of fine to coarse, dark grey to brown, feldspar-rich silty sand. Sediments composing the remainder of this unit range from dark grey silty clay to medium/medium-coarse sand. Finer segments are highly compact and dewatered. The top of Unit II, located between −6 m and −18 m MSL (deeper seaward) is identified in landward sections by the presence of organic matter (peat, root fragments, and shells in cores TJD02, TJD03 and TJD04) which is interpreted as a subaerially exposed surface.

Abundant shells and wood are present in the upper 1·5 m of this unit in TJD04 that were dated to *ca* 46 000 uncalibrated years BP. Other dates from the landward section of this unit range from 43 to >48 ka (radiocarbon dead). Although no local RSL curves for the Pleistocene exist for
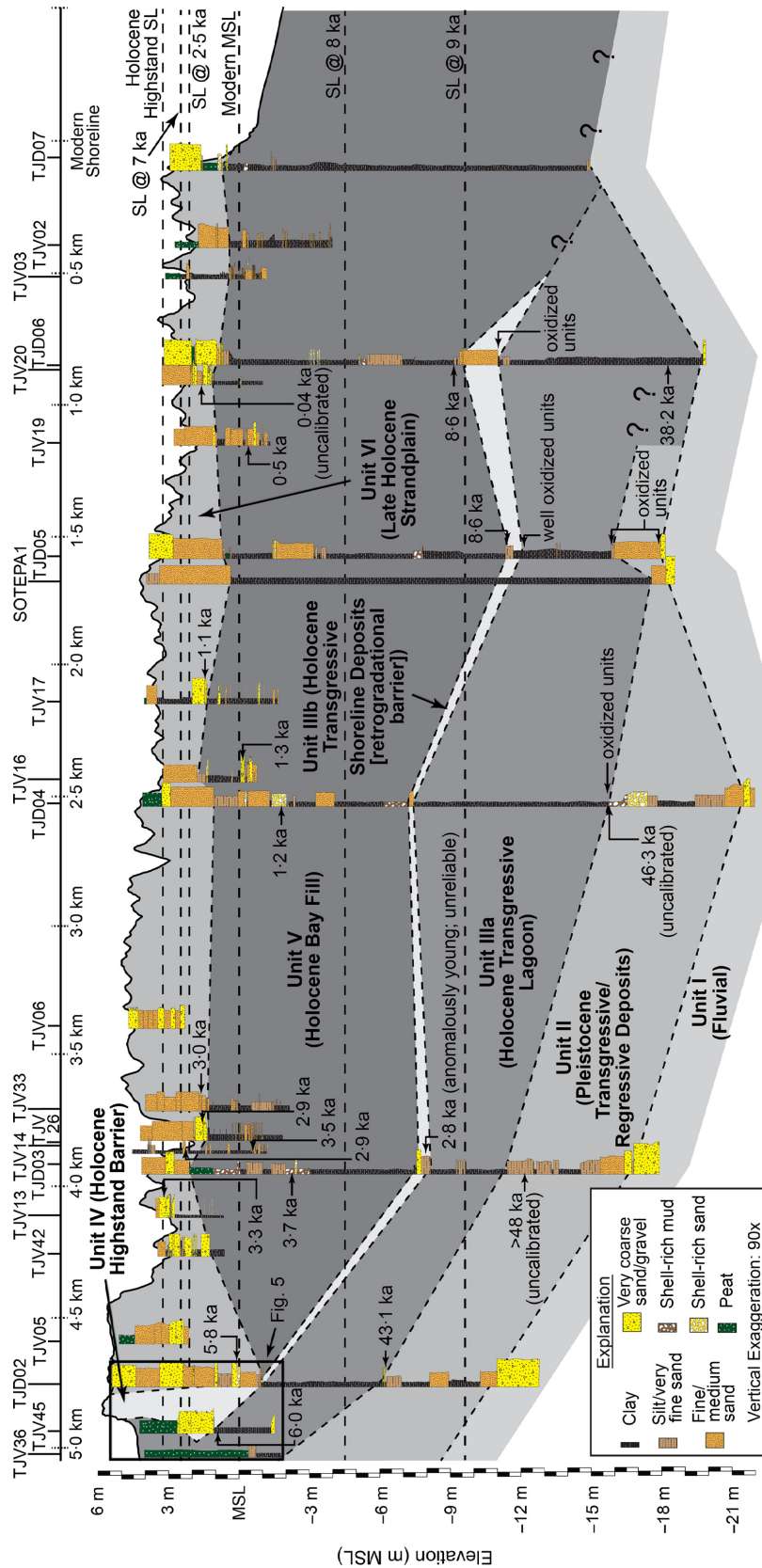
**Fig. 4.** Two-dimensional cross-shore transect of wash-boring/direct-push cores (TJD-xx), vibracores (TJV-xx) and road borings (SOTEPA1). See core locations in Fig. 3. Unless otherwise noted, all dates are calibrated 2-α ages derived from $^{14}$C dating of marine molluscs or terrestrial wood/peat/root deposits (Table 1). Palaeo-sea-level elevations are derived from model predictions (Milne *et al.*, 2005) for times before the mid-Holocene highstand and from indicator-based reconstructions (Angulo *et al.*, 2006) for the last 5800 years. Depths are given with respect to modern sea-level (MSL).

southern Brazil, eustatic sea-level at 40 to 50 ka (middle of OIS 3) was 60 to 80 m below present (Chappell, 2002; Thompson & Goldstein, 2006). Given demonstrated elevations of 120 ka shoreline deposits at or near eustatic levels in such proximal locations as Rio Grande do Sul state, southern Brazil (Tomazelli & Dillenburg, 2007), RSL at OIS 3 at Tijucas was probably in the range of −60 to −80 m MSL, far deeper than the coastal sediments of Unit II. It is therefore likely that these three dates in Unit II are all from material deposited earlier in the Pleistocene. All of these dates are near the age limit of modern radiocarbon dating and two of the three are from organic matter (roots and wood; Table 1) which is easily contaminated with younger $^{14}$C-containing carbon. Given the evidence of a coastal origin (marine shell material) and sub-aerial exposure (roots and abundant oxidation at the surface of deposits) of Unit II, it is interpreted to represent earlier transgressive/regressive coastal deposits. Although the data herein do not allow for a definitive determination of the age of these deposits, they are most logically associated with the transgressive–regressive cycle associated with the OIS 5e sea-level highstand (120 ka), when sea-level reached a maximum of *ca* 7 m MSL in southern Brazil (Tomazelli & Dillenburg, 2007).

Unit II thins in a seaward direction and is entirely absent from core TJD07 (Fig. 4). In core TJD05 and core SOTEPA1 (named for the coring company), this unit is marked by the presence of well-oxidized fine to medium sand containing rare root fragments. No such sediments were identified in core TJD06. Here, *ca* 8 m of clay to silty clay overlies the Unit I fluvial deposits. Radiocarbon analysis of wood fragments collected from −17 m MSL provided an age of *ca* 38 ka. This sample is from sediments located deeper and further seaward than other ages in Unit II. It is also not stratigraphically related to any coarser (sandy) or shell-rich beds, as is common of other ages from this unit. Thus, it is unclear if these deep, seaward deposits are associated with the Pleistocene transgressive–regressive cycle, or are a later riparian or coastal backbarrier (i.e. Unit III) deposit.

## Unit III: Early Holocene transgressive units

Unit III is sub-divided into a lower, 3·5 to 8·0 m thick, fine-grained section (Unit IIIa) composed of light grey silty clay with occasional sand stringers; and a thin (<1 m) coarser overlying section (Unit IIIb), generally composed of medium to coarse-grained sand with semi-angular granules with some shells. In TJD04, Unit IIIb is present only as organic-rich clayey very fine sand. The uppermost section of Unit IIIa is commonly well-oxidized and contains abundant root fragments.

A single radiocarbon date from this unit (TJD03-S23; 2816 ± 94 cal BP; Table 1) was collected from the slurry of the wash section of core TJD03 and, given its anomalously young age, probably originates from shallower in the section. It is thus considered unreliable. Moreover, it is anomalously young given its depth and stratigraphic relationship with an older radiocarbon date (TJD03-S16; 3710 ± 117 cal BP; Table 1) from 5·2 m shallower in the same core. This latter date corresponds well to radiocarbon dates collected from *in situ* molluscs and organic matter from proximal vibracores (Fig. 4).

Unit III is interpreted as early Holocene transgressive deposits, specifically backbarrier lagoon and peat (Unit IIIa) topped by transgressive shoreline lag deposits (Unit IIIb) (Fig. 11A). These deposits date to the rise of RSL between 9 ka and 6 ka.

Unit IIIb is likely to be the remnants of a transgressive barrier which migrated onshore by storm overwash (Fig. 11A). The onshore movement of the barrier was probably accompanied by sand deposition in the backbarrier by the flood-tidal and storm-generated currents; associated deposits are preserved as the coarser segments of Unit IIIa. These are found more prevalently in landward sections of the plain (for example, TJD02 and TJD03; Fig. 4), and are well-preserved and abundant in mid-Holocene highstand shoreline deposits.

## Unit IV: Mid-Holocene highstand deposits

In contrast to older units identified within the Tijucas Basin, sedimentary deposits associated with the mid-Holocene RSL highstand are well-preserved by subsequent progradation associated with 5500 years of RSL fall. Hein *et al.* (2014b) recognized the importance of local controls such as *upland migration potential* or UMP (controlled by shoreline wave energy and the slope and erodibility of upland surface onto which the shoreline is migrating), and longshore, cross-shore and *in situ* sediment supply rates in determining the morphology and sedimentology of highstand depositional systems. These authors also emphasized the site specificity of conditions associated with the formation of highstand

deposits within relatively small embayments in southern Brazil. Similar to these results at Navegantes Strandplain (see location in Fig. 1), the mid-Holocene highstand at Tijucas also took multiple forms. In central Tijucas, the highstand shoreline was marked by a bedrock headland which effectively split the embayment into two compartments. The resulting Type A (exposed bedrock coast; Hein *et al.*, 2014b) shoreline was characterized by waves crashing along the bedrock shore (Fig. 11B) and remained intact until the shoreline prograded eastward to, and eventually beyond, this headland. Based on the progradation curve for Tijucas (Fig. 8A), it is estimated that this occurred at *ca* 1000 BP.

The highstand shoreline in the southern compartment (southern 5 to 6 km of the modern embayment; Fig. 1B) of Tijucas was quite different. Here, the highstand shoreline was protected from dominant east to south-east wave approach by the central bedrock headland, and entirely cut off from the Tijucas River. Given dominant northerly longshore transport within the embayment, as evidenced by the paucity of sand in the strandplain or modern beach south of the Tijucas River, this southern compartment probably received little to no sediment directly from the Tijucas River between the late stages of the transgression and 1000 BP. Rather, any fine fluvial sediment (silt and clay) that reached the highstand or early regressive shorelines was first dispersed through the bay and moved onshore around the headland. The highstand here is characterized according to Hein *et al.* (2014b) as Type B (backbarrier deposits) morphology (Fig. 11B). The early post-highstand progradational ridges are nearly entirely composed of mud, making them largely indistinguishable from the highstand deposits; the highstand shoreline itself can only be identified as the location of the westernmost strandlines in maps and rare seaward-dipping reflections in mud-dominated GPR profiles.

By contrast, north-central Tijucas is located proximal to the Tijucas River and is characterized by bedrock located furthest from the modern coast. Here, the eastward-facing highstand shore was backed by erodible Pleistocene upland deposits (Asp *et al.*, 2005; FitzGerald *et al.*, 2011) and was largely exposed to waves entering the mouth of Tijucas Bay. This setting provided both a high degree of UMP and a relatively high supply of sandy sediment, an ideal environment for the construction of Type D (barrier-island complex) highstand deposits of Hein *et al.* (2014b). Indeed, sediment cores and shore-normal GPR profiles across the highstand shoreline at this location reveal a complex set of seaward-dipping and landward-dipping sandy beds, backed and underlain by mud (Unit IV; GPR Profile A; Figs 4 and 5). Together, these deposits are interpreted as a highstand barrier-island complex (Fig. 11B). This barrier was first recognized in GPR profiles and a single sediment core by Asp *et al.* (2005) and FitzGerald *et al.* (2007); additional sediment core data and a new, fully processed and topographically corrected georadar profile across this highstand barrier are presented here.

The basal unit of the highstand barrier complex is composed of silt and clay characterized in radar profiles by discontinuous, semi-horizontal reflections, probably reflecting the attenuation of radar signal by the mud (cf. Tercier *et al.*, 2000). This unit is interpreted as the landward-most section of the transgressive lagoon deposits, which merge seamlessly with the highstand backbarrier deposits landward of the highstand ridge. Radiocarbon analysis of an articulated razor clam captured in a vibracore in growth position revealed that these deposits date to 6·1 ka, corresponding to the timing of the mid-Holocene highstand in southern Brazil.

Topping these lagoonal deposits is a barrier complex consisting of a 2·2 m deep and 25 m wide semi-shore-parallel tidal channel and a 35 m wide sandy ridge composed of landward-dipping medium to coarse sandy beds. This deposition is overlain on its landward side by an 85 m long, 0·5 to 2·0 m thick, landward-thinning unit composed of landward-dipping (*ca* 2·6°), fining-upward coarse to medium sand. It has an erosional lower contact and sharp upper contact. This unit is interpreted as an overwash sequence deposited into the lagoon during the transgressive and accretionary phases of barrier migration and growth (FitzGerald *et al.*, 2007). These washovers are topped by fine, organic-rich lagoon and peat deposits (Fig. 5).

The age of the local maximum shoreline position highstand is constrained by the presence of *in situ* molluscs and peat, located within late-stage transgressive/highstand lagoon deposits and dated to between 5·9 ka and 6·1 ka (Fig. 5); both pre-date washovers associated with the growth of the highstand barrier. These lagoonal deposits reach a maximum elevation of 2·0 m MSL, but then merge seamlessly with overlying peat and modern soil horizons. Moreover, although highstand and early regressive wave-
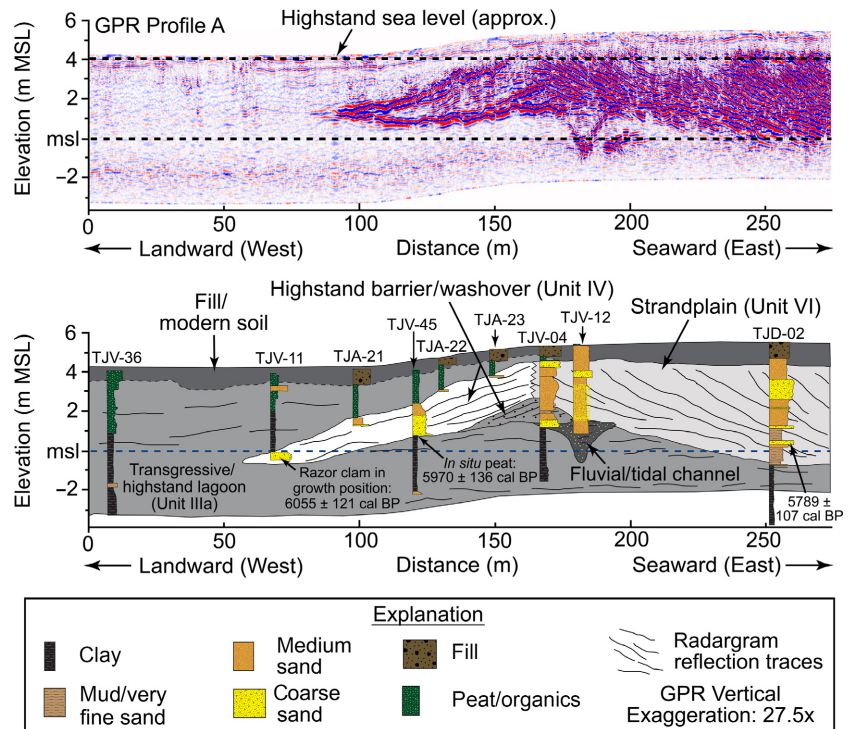
**Fig. 5.** Processed (above) and interpreted (below) ground-penetrating radar (GPR) radargram across a mid-Holocene highstand barrier ridge in central Tijucas (GPR Profile A; see Fig. 3 for location). The profile was collected along a road, accounting for smoothing of topography seen in Fig. 4. Graphic core logs from auger cores (TJA-xx), vibracores (TJV-xx) and wash-boring/direct-push core (TJD-xx) shown: msl, mean sea-level; mMSL – metres above modern mean sea-level.

built facies reach an elevation of *ca* 4·5 m MSL (Units IV and VI; Fig. 5), this elevation may be influenced by constructional wave activities (for example, construction of storm berms) that extend well above MSL at the time of deposition. The present data therefore provide little insight into the elevation of the maximum highstand shoreline. However, these data do indicate that initiation of strandplain progradation occurred between 5·7 ka and 6·0 ka, based on dates within the transgressive/highstand units (i.e. sample TJV45-S01) and within regressive (Unit IV) deposits seaward of the highstand barrier (i.e. sample TJD02-S10; Table 1; Figs 4 and 5).

Shore-parallel GPR profiles collected along the highstand ridge are characterized by subparallel horizontal reflections, indicating that subsurface reflections observed in cross-shore images represent the true dips of these transgressive, highstand and regressive/progradational shoreline deposits. Moreover, this indicates that these barrier deposits and the associated high-energy shoreline extended alongshore at least along the mapped landward-most sections of the plain. However, the lateral extents of highstand back-barrier deposits (lagoon, Tijucas River estuary) are unknown. Preliminary GPR records landward of the highstand barrier reveal a second, higher set of seaward-dipping reflections which

are interpreted by FitzGerald *et al.* (2011) as Pleistocene in age, possibly genetically related to the Pleistocene transgressive–regressive deposits (Unit II). Based on this interpretation, the Holocene highstand lagoon extends only 250 m landward of the barrier washover deposits. However, the extent and changes in dimension of this lagoon alongshore remain unknown.

Asp *et al.* (2005) suggest that, proximal to the Tijucas River, the highstand Tijucas Bay extended upstream into the river basin another >12 km landward of the identified highstand barrier system, although few details are provided as to why the estuary was mapped with this specific extent. There is a paucity of shoreline position data proximal to the Tijucas River due to removal of proximal shoreline deposits by meandering of the river in landward sections of the plain. As such, for this analyses, the present authors conservatively interpolate the highstand shoreline across the river as a curved line between mappable strandlines. However, it is possible that an estuary extended landward of this shoreline during the highstand.

Seaward of the barrier system are the oldest beach ridges of the Tijucas Strandplain; the highstand barrier grades horizontally into these seaward-dipping (5·0° to 5·3°) ridges as the shoreline shifted from retrogradational to progradational (Fig. 11C). The radiocarbon age of a mollusc shell

**Table 1.** Calibration of radiocarbon age from mollusc and peat samples collected in Tijucas, Santa Catarina, Brazil.

| Core/sample ID | Latitude (°S) | Longitude (°W) | NOSAMS accession number | Dated material | Elevation (m MSL; datum: WGS 84) | Orthogonal distance from modern shoreline (km) | $\delta^{13}C$ (‰ VPDB) | Reported age (yr BP) | Cal. 2-$\sigma$ Age (yr BP)*† | Notes |
|---|---|---|---|---|---|---|---|---|---|---|
| TJA13-S01‡ | 27·26839 | 48·73833 | OS-48421 | Mollusc | 1·20 | 1·44 | 0·3 | 1310 ± 30 | 846 ± 85 | |
| TJV11-S01‡ | 27·24124 | 48·66365 | OS-54684 | Mollusc | −0·11 | 5·05 | −0·9 | 5660 ± 40 | 6055 ± 121 | |
| TJV13-S01‡ | 27·24199 | 48·65539 | OS-54685 | Mollusc | 3·61 | 4·12 | 1·44 | 3440 ± 35 | 3303 ± 108 | |
| TJV14-S01‡ | 27·24227 | 48·65267 | OS-54686 | Mollusc | 2·32 | 3·85 | 0·67 | 3140 ± 30 | 2909 ± 114 | |
| TJV14-S02‡ | 27·24227 | 48·65267 | OS-54687 | Mollusc | −0·58 | 3·85 | 1·01 | 3590 ± 30 | 3474 ± 96 | |
| TJV16-S01‡ | 27·24415 | 48·63852 | OS-54748 | Plant/wood | −0·54 | 2·44 | −29·59 | 1500 ± 30 | 1341 ± 60 | |
| TJV17-S01‡ | 27·23038 | 48·63345 | OS-54688 | Mollusc | 1·51 | 2·15 | 0·47 | 1570 ± 30 | 1122 ± 102 | |
| TJV19-S01‡ | 27·23036 | 48·62337 | OS-54689 | Mollusc | −0·51 | 1·15 | 0·59 | 840 ± 25 | 469 ± 51 | |
| TJV20-S01‡ | 27·23077 | 48·62026 | OS-54690 | Mollusc | 1·60 | 0·86 | 1·23 | 395 ± 25 | 38 ± 50 | Invalid calib: young |
| TJV23-S01‡ | 27·24774 | 48·63164 | OS-54691 | Mollusc | −1·45 | 1·72 | 0·58 | 1520 ± 30 | 1066 ± 100 | |
| TJV25-S01 | 27·24066 | 48·66813 | OS-64792 | Plant/wood | 2·98 | 5·41 | −31·13 | 34 900 ± 820 | 39 473 ± 1894 | Landward of Holocene highstand shoreline |
| TJV26-S01‡ | 27·24226 | 48·65295 | OS-64541 | Plant/wood | 1·58 | 3·83 | 29·09 | 2830 ± 30 | 2886 ± 93 | |
| TJV28-S01‡ | 27·24226 | 48·65272 | OS-64082 | Mollusc | 2·69 | 3·80 | 0·94 | 3140 ± 30 | 2909 ± 114 | |
| TJV33-S01‡ | 27·24232 | 48·65168 | OS-64083 | Mollusc | 1·21 | 3·71 | 0·99 | 3200 ± 25 | 2990 ± 115 | |
| TJV45-S01‡ | 27·24126 | 48·66349 | OS-74112 | In situ peat | 0·90 | 4·92 | −24·72 | 5260 ± 35 | 5970 ± 136 | |
| TJV46-S02 | 27·24231 | 48·65215 | OS-74113 | Peat | 2·45 | 3·75 | −29·88 | 4250 ± 35 | 4734 ± 132 | Anomalously old; excluded from progradation curve |
| TJV47-S02‡ | 27·24234 | 48·65167 | OS-74126 | Peat/plant fragments | 2·12 | 3·77 | −28·92 | 3510 ± 30 | 3743 ± 98 | |
| TJV48-S02‡ | 27·24241 | 48·65181 | OS-74125 | Mollusc fragments | 0·31 | 3·76 | 0·68 | 3430 ± 35 | 3292 ± 108 | |
| TJV49-S02‡ | 27·24245 | 48·65154 | OS-74090 | Mollusc fragments | 2·41 | 3·74 | 0·8 | 3270 ± 35 | 3086 ± 125 | |
| TJD02-S10‡ | 27·24181 | 48·66219 | OS-67046 | Mollusc | 0·65 | 4·75 | 0·96 | 5240 ± 35 | 5789 ± 107 | |
| TJD02-S20 | 27·24181 | 48·66219 | OS-74191 | Decomposed root fragments | −5·47 | 4·75 | −29·93 | 39 000 ± 1100 | 43 060 ± 1798 | |
| TJD03-S16‡ | 27·24249 | 48·65340 | OS-67050 | Mollusc | −2·57 | 3·91 | 0 | 3780 ± 35 | 3710 ± 117 | |
| TJD03-S23 | 27·24249 | 48·65340 | OS-67048 | Mollusc | −7·74 | 3·91 | 0 | 3060 ± 35 | 2816 ± 94 | Shell sample from slurry; depth unreliable and date anomalously young |
| TJD03-S32 | 27·24249 | 48·65340 | OS-74111 | Decomposed wood | −12·54 | 3·91 | −25·84 | >48 000 | Invalid calib: old | Invalid calib: old |

**Table 1.** (continued)

| Core/sample ID | Latitude (°S) | Longitude (°W) | NOSAMS accession number | Dated material | Elevation (m MSL; datum: WGS 84) | Orthogonal distance from modern shoreline (km) | δ$^{13}$C (‰ VPDB) | Reported age (yr BP) | Cal. 2-σ Age (yr BP)*† | Notes |
|---|---|---|---|---|---|---|---|---|---|---|
| TJD04-S12‡ | 27·23045 | 48·63734 | OS-67047 | Mollusc | −1·92 | 2·53 | −3·91 | 1690 ± 30 | 1243 ± 70 | Invalid calib: old |
| TJD04-S37 | 27·23045 | 48·63734 | OS-67050 | Mollusc | −15·91 | 2·53 | 0 | 43 100 ± 1500 | 46 334 ± 2823 | |
| TJD05-S18 | 27·23039 | 48·62775 | OS-74109 | Plant roots | −10·93 | 1·58 | −27·93 | 7850 ± 35 | 8583 ± 122 | |
| TJD06-S24 | 27·23077 | 48·62032 | OS-74108 | Wood fragments | −8·71 | 0·85 | −28·38 | 7900 ± 35 | 8642 ± 194 | |
| TJD06-S38 | 27·23077 | 48·62032 | OS-74110 | Wood fragments | −17·00 | 0·85 | −26·48 | 33 800 ± 210 | 38 243 ± 627 | |

*All radiocarbon ages were calibrated using OxCal 4.2 (Bronk Ramsey, 2009) which includes a reservoir correction. Terrestrial samples (peat roots) were calibrated with SHcal13 (Hogg *et al.*, 2013) calibration curves. Marine samples (all molluscs) were calibrated using Marine13 (Reimer *et al.*, 2013), corrected to a ΔR of 8 ± 17 years, as defined in Angulo *et al.* (2005). †All dates in text are reported as 2-sigma calibrated ages before 1950. ‡Calibrated date used in construction of strandplain progradation curve (Fig. 8).

(TJD02-S10; 5789 ± 107 BP; Table 1; Figs 4 and 5) indicates that progradation had been initiated at, or soon following, the RSL highstand.

## Holocene regressive and basin-infill units

Located seaward of mid-Holocene shoreline and atop Holocene transgressive shoreline deposits are 75 km$^2$ of Holocene basin-fill (Unit V) and strandplain (Unit VI) deposits built from sediments delivered to the coast by the Tijucas River during the period of highstand and subsequent RSL fall. Basin-infill deposits (Unit V) are built upon a seaward-dipping (*ca* 0·11°) surface and have a nearly horizontal upper contact; under the area of the modern Tijucas Strandplain these deposits range in thickness from 8 to 16 m, thickening in a seaward direction. These deposits are dominantly composed of semi-compacted brown (shallower) to grey (deeper; anoxic) clay with occasional shelly layers. Sandy units, sometimes as much as 2 m thick, are common. These units are composed of sediments ranging from fine, silty, mica-rich sand in deeper sections to coarse, shelly sand in shallower sections (Figs 4 and 11C); they are interpreted as derived from flood events of the Tijucas River, which delivered abundant coarse material to the fronting bay. All shell and organic materials collected from within this unit date from the middle to late Holocene (Fig. 4; Table 1). These materials have an overall trend of decreasing age towards the coast, as is expected in a progradational sequence.

Overlying the basin-fill deposits is the Tijucas Strandplain (Unit VI), composed of seaward-dipping sandy (fine to coarse sand) and muddy (dominantly semi-compacted silty clay) strata interpreted as beachface and foreshore deposits associated with the progradation of beach/dune ridges and cheniers during strandplain construction. The point of transition between a 'prograded' barrier, formed in a regime of stable or rising RSL, and a 'regressive' strandplain, formed by forced regression (Roy *et al.*, 1994), is unclear. The timing of onset of progradation (5·7 to 6·0 ka) is well within estimates of the timing of the RSL highstand (5 to 7 ka), and *ca* 1000 years earlier than the earliest estimate for the timing of RSL fall in Santa Catarina (Fig. 2). Thus, it is likely that earliest progradation of the Tijucas Strandplain (Unit VI) was driven by abundant sediment derived from the Tijucas River as part of a *highstand systems tract* during a period of *normal* regression. This was followed by strandplain progradation caused by

the onset of slow RSL fall and an abundant supply of sediment; thus the strandplain represents a condition of both *normal* and *forced* regression. Such a delay in baseline fall following the onset of regression is well described in the sequence stratigraphic literature (cf. fig. 3.19 of Catuneanu, 2006).

The progradational/regressive strandplain surface is relatively flat with a low, seaward-dipping gradient and a relief of generally <1 m (Fig. 4). Subsurface beach/dune ridges dip at 8° to 11°. Muddy sections are generally flat lying and transparent in GPR profiles (Fig. 6). South of the Tijucas River, the strandplain is largely mud-dominated with only rare, thin, sandy (fine silty sand) layers. Both sand and mud layers are occasionally truncated by more steeply dipping clinoforms in GPR radargrams. In the proximal strandplain at Navegantes (Fig. 1), these have been correlated with heavy mineral lag deposits associated with infrequent (*ca* 900 to 2000 year return interval) storm events (Buynevich *et al.*, 2011). Shore-parallel GPR profiles are characterized by parallel, horizontal reflectors, indicating that true dips of strandplain deposits are captured in shore-normal profiles.

Individual clinoforms within sandy sections of the strandplain have an average spacing of *ca* 1 m (Figs 5 to 7); given the 5 km width of the plain and its period of deposition during a 5800 year period, this corresponds to time-averaged pseudo-annual deposition. Individual clinoforms are further interpreted as summer–winter couplets in sediment grain size and heavy mineral composition (FitzGerald *et al.*, 2007).

## TRENDS IN MID TO LATE-HOLOCENE PROGRADATION

Following the mid-Holocene highstand, falling RSL combined with abundant sediment derived from the Tijucas River forced shoreline progradation and the development of the gently (0·05°) seaward-dipping Tijucas Strandplain. Several distinct shifts in progradation style during this period of time are identified in geophysical, sedimentological and chronological data.

### Trends in strandplain sedimentation and beachface morphology

The strandplain can be divided into two sectors: a mud-dominated southern sector and a mud-rich, sand-dominated northern sector.

### Mud-dominated southern plain

South of the Tijucas River, the strandplain is composed almost entirely of silty clay, with rare silty fine to medium-grained sand beds. Model simulations have demonstrated that this region experiences very low wave energy (Asp *et al.*, 2005; Hein *et al.*, 2015). Sandy units in the southern sector are rare and thin, indicating deposition from very short-lived processes. These are most likely to be derived from a combination of: (i) local sedimentation from the Inferninho River; (ii) large flood events on the Tijucas River that delivered abundant sandy deposits to the coast; and (iii) periods of intense shoreface reworking during periods of high wave energy during storm events.

More than 10 years of observation of the Tijucas coast provide insight into the processes by which each of these proposed mechanisms would act. For example, although winter storms along the relatively-quiescent coast of central Santa Catarina are generally small in magnitude, two recorded tropical cyclones have impacted this coastline in >100 years: Cyclone Catarina in 2004 (McTaggart-Cowan *et al.*, 2006) and Tropical Storm Anita in 2010. Neither event was observed to have left any discernible sedimentological signature at Tijucas, probably due to the high degree of wave protection afforded by the shallow offshore, muddy water in the bay, and fronting headlands and bedrock islands (Fig. 1B). Nonetheless, it is highly likely that waves associated with these high-energy events remobilized some coarse sediment in the nearshore, allowing it to be re-distributed alongshore and/or into deeper parts of the bay.

In November 2008, the Santa Catarina coast was impacted by a severe flood event that resulted in the nearby Itajaí River reaching a flood stage of 11·5 m above normal (Desastre, 2008) and the mobilization of large quantities of sediment in the form of widespread landslides in coastal catchments. This resulted in the deposition of a *ca* 30 cm thick sand lens along the typically mud-dominated intertidal zone along the beach in the northern sector of Tijucas. Four months later (March 2009; Fig. 1C), a shallow auger core extracted from this area revealed that this sand had been covered by mud, leaving a thin (<25 cm) sand lens similar in thickness to sand lenses documented in the muddy strandplain in the southern sector of the river. It is noted that either of these same processes (high-energy events or floods) is also likely to explain the derivation of the sandy beds observed

within the basin-fill sequence (Unit V) north of the Tijucas River (Fig. 4).

A final explanation for the origin of these thin beds is avulsion of the Tijucas River. However, the presence of continuous strandlines (palaeo-shorelines) to within 250 m (shore-parallel) of the modern river across the strandplain attest to the low degree of avulsion and migration of the Tijucas River during the period of progradation.

### Sand-dominated northern plain

North of the river and extending 100 to 300 m south of the river, the strandplain is composed of sandy, muddy and alternating sand/mud sections. Sandy sections are as much as *ca* 7 m thick. The gross composition of this region was first described by Buynevich *et al.* (2005) and FitzGerald *et al.* (2007). However, new data presented here provide further insight into the textural patterns of this system and associated forcing mechanisms.

Shore-normal radar profiles collected along two semi-parallel transects in the northern sector (Fig. 6) indicate a gradual change in sedimentary composition of the plain with time. In its landward-most sections, this sector is composed of a set of semi-parallel, seaward-dipping beds that extend uninterrupted for *ca* 700 m (Fig. 7A). Composed of medium to coarse-grained sand, these beds dip seaward at an average of 10·6° (Fig. 7C). Further seaward, mud deposition gradually becomes an important component of the plain (Fig. 11C to E). Here, 3 to 5 m thick sandy strandplain segments alternate with pure muddy segments. Sandy sections are composed of medium sand and dip seaward at an average of 8·1° (Fig. 7C).

Continuous sand-dominated and mud-dominated segments extend tens of metres to >100 m in a cross-shore direction. Furthermore, individual sand and mud complexes can be traced for more than 6 km shore-parallel across the plain (Fig. 6), which is consistent with the length of individual shoreline strandlines observed in vertical aerial photographs. Periods of sand deposition are characterized by pure sand with little to no mud, whereas muddy periods are marked by rapid transitions between sand and mud deposition (Fig. 6). The mechanism for this alteration in sedimentation regime is the subject of ongoing investigation. It is hypothesized that these transitions are related to persistent compositional changes in the Tijucas River sediment load, a function of both the transport capacity of the river (flow rate) and the sediment available in the basin for export. In this manner, these compositional changes may result from basin-scale landscape responses to extrinsic [for example, climate (precipitation) change] and intrinsic (for example, erosion and landsliding) forcings during the middle to late Holocene.

The modern upper shoreface at Tijucas has a slope of 0·5° to 1·0° and is dominated by mud and fluidized mud (Buynevich *et al.*, 2005; Schettini *et al.*, 2010) which extend to the upper intertidal zone. The upper beachface is defined by a thin (<30 cm) berm composed of medium to coarse-grained sand which has a slope of <5° (Figs 1C and D) and is backed by a *ca* 1 m high sandy foredune ridge. This sandy section of the beach reflects reworking during high-energy conditions and is likely to be preserved as the most recent in a series of thin, widely spaced, storm-built cheniers (mud-encased reworked sand ridges) that extend 1·2 km inland (Fig. 6). Sandy units in the seaward section of the plain are thin (<3 m thick; Fig. 7B) and rare. Where present, they are composed of fine to medium seaward-dipping (average of 10 measurements: 7·0°) beds.

### Strandplain depositional trends

Overall, several distinct trends can be identified in the northern sector of the Tijucas Strandplain. There has been a clear shift from a sand-dominated to a mud-dominated shoreface (Fig. 6). For the first *ca* 2000 years following the mid-Holocene highstand the beachface and nearshore were entirely composed of a thick sand-dominated sequence built atop muddy bay-infill sediments. This composition gradually shifted to mixed sand and mud, and, in the last *ca* 1000 years, nearly entirely mud. Moreover, sandy segments of the strandplain have become thinner and finer in texture through time, decreasing from 7 to 8 m of coarse sand in the the landward-most sections to 2 to 3 m of fine to medium sand in the seaward-most sections. Additionally, beachface slopes have gradually decreased from >10° in landward sections of the plain to *ca* 8° mid-plain, to only *ca* 7° proximal to the modern coast.

Relationships between equilibrium beachface slopes and grain size indicate that a decrease in grain size corresponds with an increase in beachface–slope ratio (i.e. a decrease in slope). Moreover, for a given particle size, a more exposed beach (or one during initial stages of a

**Table 2.** Summary of changes in strandplain progradation associated with bay infilling at Tijucas Strandplain, Santa Catarina, Brazil.

| | Holocene highstand (5800 BP) | 2500 BP | 1000 BP | Modern |
|---|---|---|---|---|
| Sea-level (m MSL) (mid-point of Angulo *et al.* (2006) northern S.C. envelope) | 3·1 | 2·2 | 1·4 | 0 |
| Beachface and shoreface sediment type | Coarse sand | Alternating sand (medium) and mud | Mud with fine to medium sand cheniers | Mud-dominated with medium to coarse sandy beachface |
| Orthogonal distance shoreline prograded in north-central Tijucas since mid-Holocene highstand (m) | 0 | 1475 | 3175 | 4850 |
| Strandplain area (km$^2$) | 0·0 | 20·0 | 50·8 | 74·3 |
| Time-integrated strandplain area growth rate (km$^2$ kyr$^{-1}$) since mid-Holocene highstand | 0·0 | 6·1 | 10·6 | 12·8 |
| Volume of mid to late Holocene sediments deposited between highstand shoreline and modern 10 m bathy (km$^3$) | 0·00 | 1·34 | 1·74 | 2·65 |
| Sediment deposition rate (km$^{-3}$ kyr$^{-1}$) from prior timeslice shoreline to modern 10 m bathymetric contour | 0·0 | 0·4 | 0·3 | 0·9 |
| Thickness of sandy strandplain deposits (m) | 7 to 8 | 4 to 5 | 2 to 4 | 2 to 3 |
| Beachface slope (°) | 10·6 | 9·0 | 8·0 | 7·0 |
| Shoreface slope (°) | 0·109 | 0·084 | 0·073 | 0·067 |
| Shoreline progradation rate (m yr$^{-1}$) | 0·4 | 0·7 | 1·5 | 1·8 |
| Significant wave height (Hs) (m) | 1·81 | 1·65 | 1·53 | 1·24 |
| Onshore wave energy transport at shoreline (kW m$^{-1}$) | 18·0 | 9·0 | 7·0 | 4·0 |

storm) will tend to be flatter than a beach experiencing lower wave energy (Wiegel, 1964; Fig. 7C). The beachface evolves towards equilibrium with the incident wave energy, which is affected by both the nearshore/offshore slope and refraction and diffraction processes. Therefore, beachface–slope ratios in sediments of known texture can be used to reconstruct relative temporal changes in incident wave climate.

It is expected that the beachface at Tijucas slope would decrease in a seaward direction due to the general fining trend across the plain. However, that decrease is less than expected based on established relationships (Fig. 7C). This is in spite of the fact that earlier in the history of plain evolution, the shoreline was longer and irregular, which would have produced some loss of incident wave energy due to refraction and diffraction. Thus, the Tijucas beach is

clearly responding to an additional forcing beyond changes in grain size and shoreline length and configuration. A shoaling of the nearshore region during the RSL fall is a possible explanation for the observed trend.

## Changes in progradation rates

A subset of calibrated radiocarbon (2-α) ages for 21 samples collected from the shallowest sections of all cores across the Tijucas Strandplain were used to provide insight into changes in the rate of shoreline progradation during the period of strandplain growth (Table 1) through the generation of a progradation curve for the northern sector of the strandplain (Fig. 8A). The data set herein includes several minor reversals (younger ages landward of older dated material) in dates derived from shell hash, demonstrating the need

for care in interpreting chronologies from radio-carbon dating of possibly reworked materials (Oliver *et al.*, 2015). Nonetheless, the resulting curve is quite remarkable, demonstrating a strong trend of gradually accelerating shoreline progradation, even when accounting for ^{14}C error and uncertainty due to reversals. In the first 2500 years following the mid-Holocene highstand, the shoreline prograded at a time-averaged rate of 0·4 m yr$^{-1}$. This increased to 0·7 m yr$^{-1}$ during the accretion of the mid-plain, and as much as 1·8 m yr$^{-1}$ in the last 1500 years (Fig. 8A).

Similar trends are also evident when changes in shoreline shape are taken into account. For example, for a given sediment supply volume, an extension into a progressively narrowing embayment would cause a shortening of the shoreline and acceleration in progradation rate. The Tijucas Strandplain not only grew seaward faster through time, but its aerial growth also accelerated, from 6·1 km$^{-2}$ kyr$^{-1}$ in the first 2500 years, to 20·5 km$^{-2}$ kyr$^{-1}$ between 2500 BP and 1000 BP, and then to 23·5 km$^{-2}$ kyr$^{-1}$ in the most recent 1000 years (Table 2). Thus, the observed acceleration in progradation cannot be accounted for by a shortening of the shoreline alone.

### Changes in wave energy

Hydrodynamic modelling of the Tijucas Basin suggests an expected close temporal relationship among sediment infilling, gradual reduction in wave energy and long-term decrease in sand abundance along the prograding shore. Wave-energy conditions in Tijucas embayment are depicted for four time periods beginning at the Holocene highstand and extending to the present shoreline condition (Fig. 10A). A representative profile across the embayment, just north of the present river mouth, reveals spatial and temporal changes in bay infilling, significant wave height and onshore wave-energy transport (Fig. 10B and C). Significant breaker height values were calculated using a breaker height/depth equal to 0·6. The bathymetric profiles demonstrate that, coincident with bay infilling and seaward progradation of the shoreline, was a more than four-fold decrease in onshore wave-energy transport from 18 to 4 kW m$^{-1}$. This effect is driven by changes in bathymetry between each studied timeslice: bay shoaling along with a decrease in nearshore slope (0·11° at 5800 BP to 0·07° at present) resulted in a reduction of significant breaker height from 1·81 m in 5800 BP to the present 1·24 m. These results thus demonstrate a strong correlation between shallowing of the bay and dissipation of wave energy, suggesting a role of internal dynamics driven by bay infilling in the variability observed across the Tijucas Strandplain. Notably, the largest difference in wave energy occurred between 1 ka and present, the same time period when the beachface and intertidal zones at Tijucas shifted to a dominantly muddy regime (Fig. 6). It is also important to note that shoaling in the nearshore caused large waves to break increasingly further offshore, such that at the present time they break many hundreds of metres offshore of the mud beach.

## MECHANISMS RESPONSIBLE FOR OBSERVED TRENDS IN SYSTEM EVOLUTION

A total of *ca* 2·7 km$^3$ of sediment was deposited between the Tijucas Bay mid-Holocene high-stand shoreline and the modern 10 m bathy-metric contour in the past 5800 years. Time-averaged rates of sediment deposition were highly variable: 0·4 km$^{-3}$ kyr$^{-1}$ between the mid-Holocene highstand (5800 BP) and 2500 BP, 0·3 km$^{-3}$ kyr$^{-1}$ between 2500 BP and 1000 BP and 0·9 km$^{-3}$ kyr$^{-1}$ during the last 1000 years (Table 2). These variable accumulation rates are more likely to be reflective of the assumptions and errors inherent in the palaeo-bathymetric reconstructions and are best considered as order of magnitude estimates, because there is no available independent proxy of sediment delivery rates to this embayment.

Fine-grained sediment dominates sediment discharge of the Tijucas River, as indicated by the preponderance of mud both spatially and vertically in the basin and by the plumes of mud extending several kilometres offshore from the river mouth during flood events. Despite this dominance in mud source, 8 m thick sand units were deposited along the northern plain following the Holocene highstand (Fig. 6). Sand has decreased in prevalence with time and across the plain, giving way to mud that pervades the present beach and nearshore zone. The near-shore sedimentation history of the plain reflects wave energy that has drastically reduced during the past 5800 years due to basin filling and near-shore shoaling. Specifically, several interrelated changes occurred during the period of simulta-

neous infilling and progradation (Table 2): (i) the upper shoreface and beach shifted from sand-dominated to mud-dominated (Fig. 6); (ii) strandplain deposits gradually thinned from 7 to 8 m to 2 to 3 m thick (Fig. 6); (iii) the sandy lithosome gradually fined from medium to coarse sand to fine to medium sand; (iv) beachface slopes gradually flattened from >11° to *ca* 7°, decreasing less than expected given the associated change in grain size (Fig. 7); (v) strandplain progradation accelerated from 0·4 to 1·8 m yr$^{-1}$ as RSL fell gradually and linearly (within error envelopes) (Fig. 8B); and (vi) incident wave energy gradually decreased from 18·0 to 4·0 kW m$^{-1}$ during the same time span (Fig. 10).

Taken independently, each of the observed changes across the Tijucas Strandplain can be explained, in part, by one or more alternative allogenic or autogenic mechanisms; several of these are described in detail below. However, only one, autogenic basin infilling, can explain the observed stratigraphy at Tijucas and all of the numerous sedimentological, morphological and chronological trends observed across the plain.

### Allogenic sea-level change

Relative sea-level changes may also account for a sub-set of the trends observed for Tijucas in the past 6000 years. According to palaeo-sealevel reconstructions based on empirical data sets (Angulo *et al.*, 2006) and glacio-hydro-isostatic model predictions (Milne *et al.*, 2005), RSL in central Santa Catarina reached its highstand elevations between 4 ka and 7 ka (Fig. 2). The mid-point of the highstand in the RSL-change envelope for northern Santa Catarina is 3·1 m MSL (Angulo *et al.*, 2006). A 3·1 m fall in RSL from that highstand elevation to modern during the period of progradation (average rate of *ca* 0·6 m kyr$^{-1}$) would have played a clear role in the reduction of bay accommodation at Tijucas. However, given a thickness of Holocene infill deposits below modern MSL at the modern Tijucas shoreline (TJD07, Fig. 4) of 14·9 m, RSL fall only accounts for 17% of the decrease in depth of the bay. The remaining accommodation loss (>80%) is attributed solely to infilling by mud.

Relative sea-level fall may also partially explain observations of accelerating progradation, at least for the early part of the record. Following the RSL reconstructions for central or northern Santa Catarina of Milne *et al.* (2005) or

Angulo *et al.* (2006), RSL fall did not begin in earnest at Tijucas until *ca* 5 ka. Based on this estimate and the reconstructed progradation curve (Fig. 8B), it can be assumed that the transition between a normal regressive phase (prograding barrier) and forced or mixed regression (strandplain formation) occurred following deposition of the landward-most *ca* 500 m of the strandplain. Driven solely by shoreface and beachface sediment deposition, early progradation would have proceeded slower than later periods in which depositional regression was supplemented by downstepping associated with RSL fall. However, this observation cannot alone account for the continued acceleration in progradation following the onset of RSL fall (Fig. 8B).

### Allogenic changes in sediment supply

The sediments comprising the Tijucas Strandplain were derived either from offshore sources via longshore and cross-shore sediment transport, or from upland sources via the Tijucas River, which discharges into the centre of the modern bay. Long-term, unidirectional changes in the rates of delivery of sand or mud from these two sources could explain some (for example, gradual decrease in strandplain sand content) of the observed cross-shore trends within the Holocene regressive lithosome.

For example, reversals in longshore transport directions have impacted depositional patterns along other sections of this coast by changing relative rates of sand delivery (e.g. Dominguez *et al.*, 1987). Such processes would require a dominant reliance on shelf sediment in the development of a coastal system; this is the case for much of the southern Brazilian coast. For example, Hein *et al.* (2013) found that the nearby 40 km$^2$ Pinheira Strandplain was formed almost entirely from shelf-derived sediments. In fact, the Rio de la Plata, located >1000 km south of central Santa Catarina, has been identified as the likely ultimate source of sediment for the Rio Grande do Sul and southern Santa Catarina coasts (Dominguez *et al.*, 1987; Cleary *et al.*, 2004; Martinho *et al.*, 2008). However, the Tijucas Strandplain is fronted by bedrock headlands and, to the south, a large Santa Catarina Island (Fig. 1); together, these interrupt regional northerly longshore sediment transport, effectively prohibiting the accumulation of abundant shelf sediments in Tijucas Bay. Moreover, sediments originating from offshore are expected to be tex-
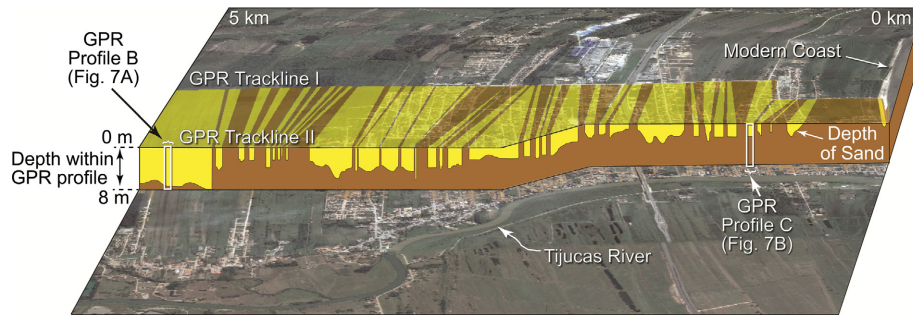
**Fig. 6.** Three-dimensional perspective derived from parallel shore-normal ground-penetrating radar (GPR) profiles across the plain. These are used to map the composition of the upper 8 m and show transitions between sandy and muddy sections of plain within an overall trend of thinning of the strandplain sequence and decrease in its sand content in a seaward direction. Yellow: sand; Brown: mud. Vertical exaggeration: *ca* 40×.

turally and mineralogically mature, with carbonate derived from shelf sources, but little mud (Tillman & Siemers, 1984). These characteristics do not match those of the sediments comprising the Tijucas Strandplain or bay-infill sequences, which are highly heterogeneous and relatively compositionally immature. These observations support the conclusions of Schettini *et al.* (2010), which demonstrate that the Tijucas River is the nearly singular sediment source in the modern bay. Thus, if changes in sediment inputs are responsible for the predictable pattern of sediment portioning in the Tijucas Strandplain, then it must be driven by long-term changes in the sediment delivered by the Tijucas River.

Although highly variable, millennial-scale sediment accumulation rates show no unidirectional increase (Table 2), which would be required to account for the increased rate of progradation through time; rather these vary between $0.3$ km$^{-3}$ kyr$^{-1}$ and $0.9$ km$^{-3}$ kyr$^{-1}$. These accumulation rates even decrease during a period (2500 BP to 1000 BP) when progradation rates more than doubled. Thus, there is no evidence to support increased sediment discharge to the embayment as a responsible mechanism for the observed changes in progradation rate.

Natural climate changes in the Tijucas Basin could also control the relative rate of sand and mud delivery to the Tijucas coast, possibly explaining the shift from a sand-dominated to mud-dominated coast. In fact, the present authors hypothesize that it was high-frequency climate changes which are responsible for changes in the relative bedload and suspended load export rates and, therefore, for the rapid sand–mud transitions observed in the central

4 km of the plain (Fig. 6). Holocene changes in the regional climate system encompassing the Tijucas River basin have been linked to fluctuations in the intensity of the South America Summer Monsoon (SASM), which are in turn driven by changes in austral summer insolation, El Niño-Southern Oscillation (ENSO), Pacific Decadal Oscillation (PDO), tropical Atlantic variability, Northern Hemisphere temperatures and Atlantic Multidecadal Oscillation (AMO) over interannual to millennial timescales (see Vuille *et al.*, 2012, for a review summary). Holocene climate records derived from speleothems, as well as lake and ice cores, indicate that the early to middle Holocene was warmer and drier than present (e.g. Gouveia *et al.*, 2002; Cruz *et al.*, 2007, 2009; Prado *et al.*, 2013). This period was followed by several millennia of enhanced moisture availability via a strengthening of the SASM starting at 5 to 3 ka, transitioning to a relatively cool and moist regime during the last 1000 years, with some short-term variability around the Medieval Warm Period and Little Ice Age (Behling, 1995; Seltzer *et al.*, 2000; Behling *et al.*, 2004; Martinho *et al.*, 2008; Leonhardt & Lorscheitter, 2010; Vuille *et al.*, 2012).

The mechanisms by which such climate changes would be transferred to depositional trends in the coastal system are complex, driven by terrestrial processes such as erosion and weathering, which are, in turn, highly sensitive to forcings including rainfall, temperature and vegetation changes (cf. Bull, 1991; Tucker & Singerland, 1997; Thomas, 2003). For example, the overall humidification of the Tijucas Basin may have increased overland flow and erosion rates, thereby enhancing sediment export to the coast; this may in fact explain the potentially high rates of sediment accumulation in the bay
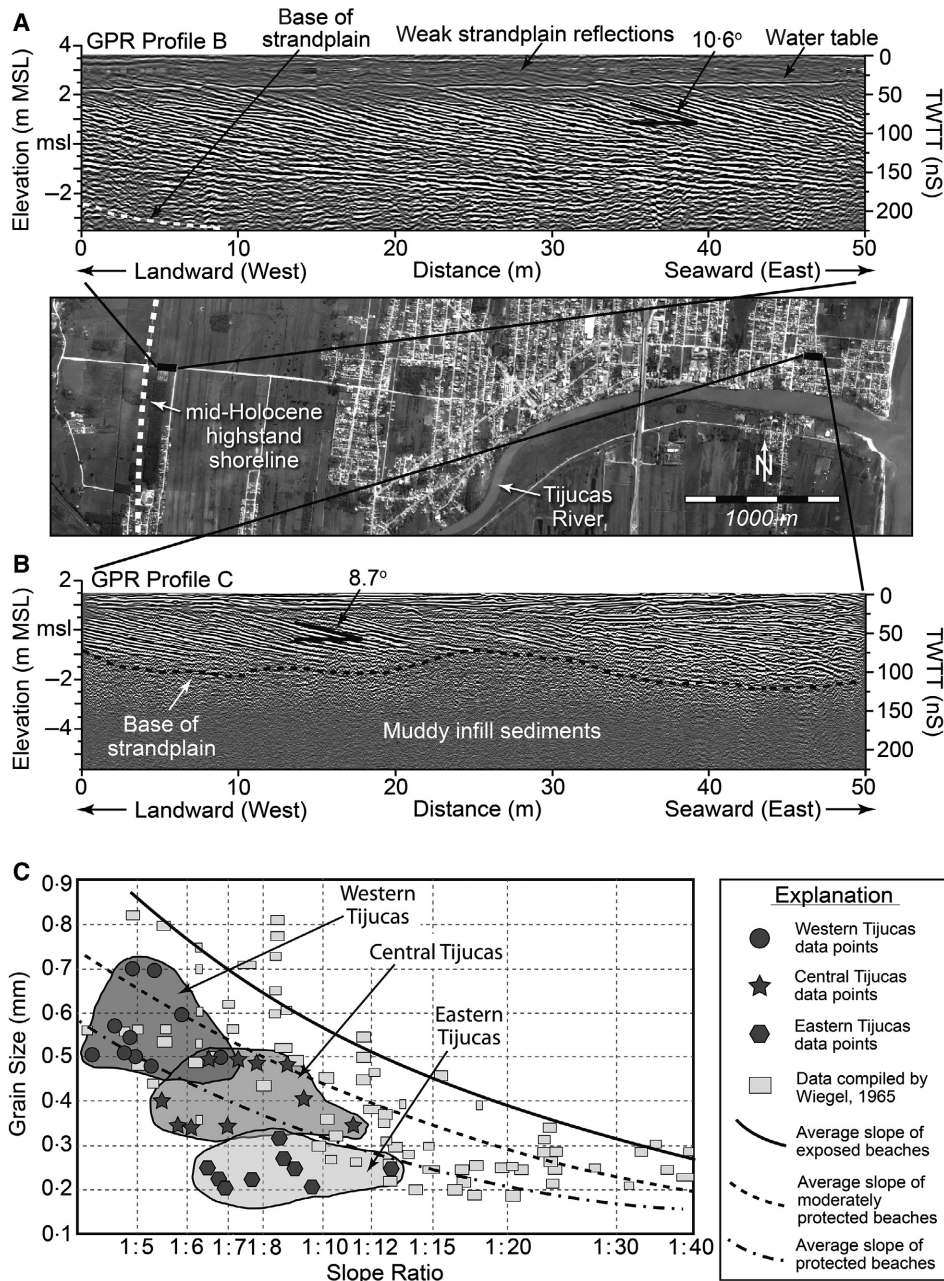
**Fig. 7.** Changes in beachface slope across the Tijucas Strandplain: mMSL, metres above modern sea-level; TWTT, two-way travel time. (A) GPR Profile C, collected *ca* 200 m seaward (east) of the mid-Holocene highstand barrier in a sand-dominated section of the plain. (B) GPR Profile D, collected *ca* 650 m landward (west) of the modern shoreline in a sandy section of the mud-dominated eastern plain. Note that both profiles are identically processed and have the same horizontal and vertical scales. Note the gentle shallowing of shoreface reflectors and the thinning of sandy strandplain units as mud-dominance increases in a seaward direction. Vertical exaggeration of both profiles is the same, 1·1×. (C) Slopes of sandy beachface (strandplain) GPR reflections (10 measurements from GPR profiles from each region) and associated sediment grain sizes from across the Tijucas Strandplain plotted on data compilation of Wiegel (1964).

during the last 1000 years (Table 2). However, counteracting this effect, wetter conditions could be linked with changes in vegetation patterns (Behling, 1995) which may have reduced soil erosion and associated sediment export rates, except during periods when the saturation threshold is exceeded. Nonetheless, even if terrestrial climate changes are in part responsible
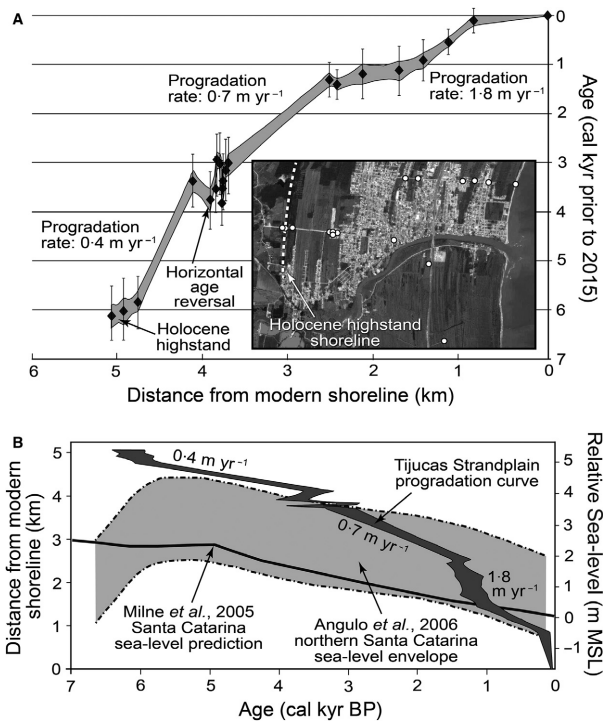
**Fig. 8.** Variability in progradation rate across the Tijucas Strandplain. (A) Progradation curve plotted against cross-shore distance, based on 20 calibrated radiocarbon dates (2-α error bars) collected across the plain and modern shoreline and calculated using Clam 2.1 age–depth modelling software (Blaauw, 2010). Locations of cores from which dates originate are shown as white circles in inset map. Distances are measured as orthogonal from the shoreline, reflecting the contemporaneous progradation of curvilinear shorelines. Grey envelope is the 95% confidence interval of linear interpolation between dating points. Horizontal age reversals denote locations where younger dates were recorded landward of older dates. Note the temporal acceleration in progradation. (B) Progradation curve re-plotted against time and in comparison to the relative sea-level (RSL) curve for northern Santa Catarina (Angulo *et al.*, 2006). Note the accelerating progradation during a period of gradual, linear (within error envelopes) RSL fall.

for increased mud delivery to the Tijucas coast, this leads to the same overall pattern of basin infilling with mud, and the attendant decrease in accommodation and strandplain thickness, and accelerating progradation rates captured by the present data. Thus, although trapping of mud within the bay is the most plausible explanation for the trends observed at Tijucas, allogenic changes in sediment supply due to climate change may have played a secondary role. A more complete investigation of how any such

climate signals would have been incorporated within the Tijucas Strandplain is clearly required to understand primary or secondary (i.e. short-term sand–mud transitions of Fig. 6) mechanisms by which regional climate change impacts coastal sedimentation. The findings herein demonstrate that a similar approach should be applied to other physiographically similar coastal regions around the world, as well as strandplain sequences in the rock record.

## Autogenic estuary infilling and shifting depocentres

During late-stage transgression and highstand, fluvial mud would have been largely deposited in an estuary formed from the flooding of the lower Tijucas River, and in the backbarrier of retrograding shoreline deposits. Based on sparse preliminary data, Asp *et al.* (2005) attributed the gradual increase in mud in Tijucas to the filling of a broad estuary of the Tijucas River. According to this hypothesis, infilling of the estuary in the late Holocene allowed more mud to be delivered to the nearshore and shoreface (Asp *et al.*, 2005). However, there is no evidence for the presence of such a broad estuary landward of the mapped highstand shoreline. Moreover, the initiation of RSL fall at 5 ka would have immediately shifted the depocentre for the fine-grained fraction offshore into Tijucas Bay, as the mouth of the Tijucas River migrated seaward and fluvial incision began in response to falling base level (cf. Blum & Törnqvist, 2000).

Nonetheless, this hypothesized shift in depocentre for muddy sediments from an estuary to the shoreface may indeed be partially responsible for the change to a mixed sand and mud plain. It is noted that this sedimentological transition occurred at *ca* 4 ka, soon following the onset of RSL fall. However, erosion of sandy upland (Pleistocene) or earlier strandplain deposits associated with downcutting would also have allowed for enhanced sand delivery into the bay. Moreover, this mechanism was a one-time event and cannot explain the continued shift towards a mud-dominated regime, nor the continued decrease in wave energy. Thus, whereas a shift in depocentre early in the period of progradation is possible, it would only be a contributing factor to the overall nearshore mud deposition and attendant decrease in accommodation responsible for the overall trends observed in Tijucas.
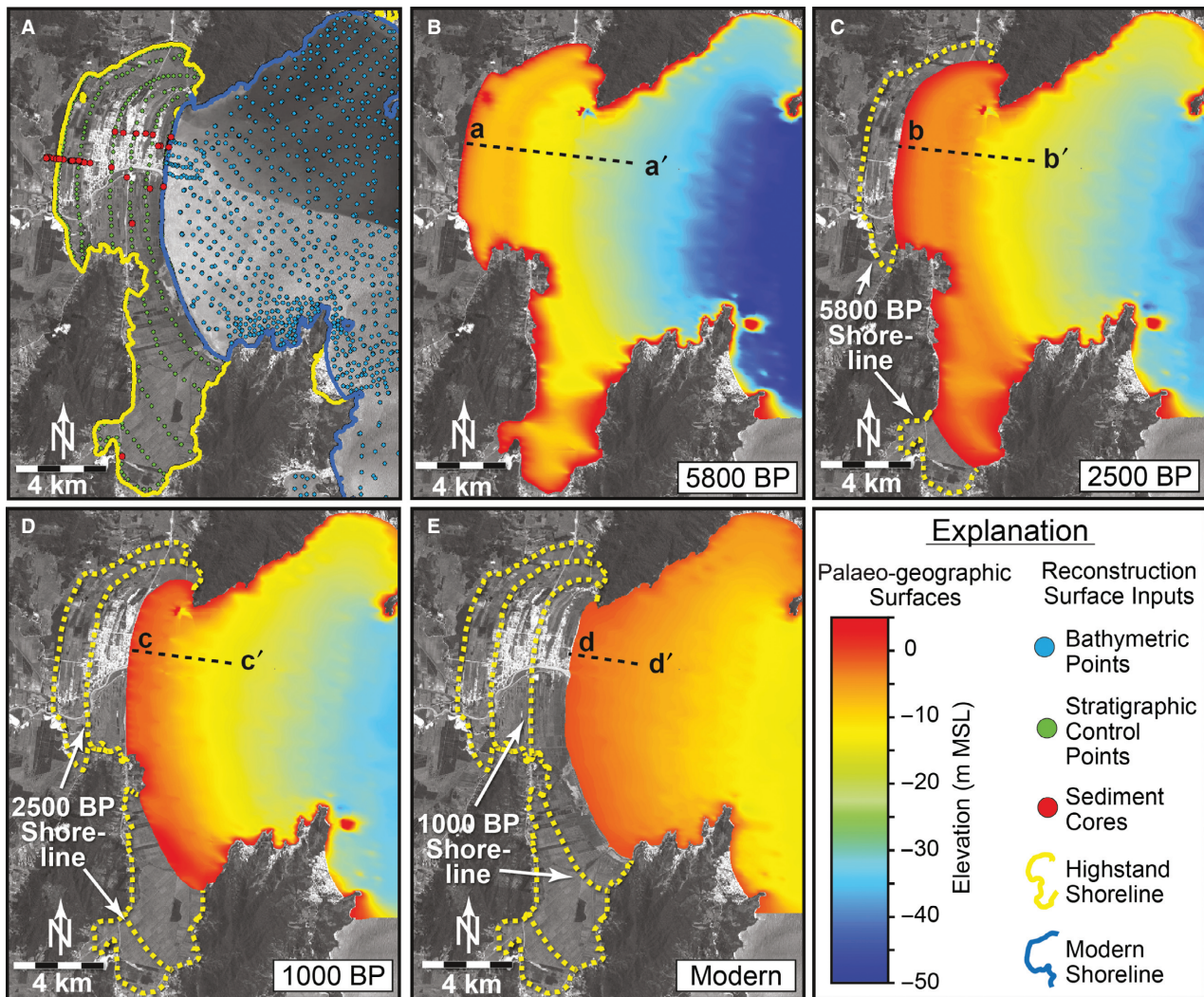
**Fig. 9.** Paleaogeographic reconstructions of Tijucas Bay based on modern bathymetric data, core-long stratigraphy, control points positioned along palaeo-shorelines of sediment cores and palaeo-shoreline positions (A). Bay bathymetry is calculated for (B) the mid-Holocene highstand; (C) 2500 BP; (D) 1000 BP; and (E) the modern bathymetric surface. Surfaces are constructed based on core stratigraphic data (onshore of modern shoreline) and modern bathymetric data (offshore of modern shoreline). All surfaces share the same bathymetric colour scale.

## Autogenic shoreline geometric changes

The findings of this study show that the Tijucas Bay shoreline has changed its length, shape and continuity during the period of progradation. It has become more exposed to ocean swell as it has prograded (Fig. 9B to E). Moreover, progradation shortened the shoreline, thereby decreasing the area of wave action and, other factors being equal, increasing the per unit area wave energy. Hence, the observation of Tijucas growing more 'protected' during the period of progradation (Fig. 7C) cannot be explained by changes in the protection afforded by fronting headlands as the shoreline shape and orienta-tion changed. Rather, the smaller than expected decrease in beachface slope reflects internal wave dampening processes through wave inter-action with a shallowing bay and fluid mud in the shoreface.

## Anthropogenic impacts

Following initial European settlement of south-ern Brazil in the late 17th Century, vast areas of Atlantic pluvial forest (the dominant vegetation type in the Tijucas Basin) in eastern Santa Cata-rina state were deforested with the expansion of colonization in the 1800s (Behling, 1995). More

recently, expansive mining operations in the Tijucas River floodplain have removed large quantities of medium to coarse sand, although Buynevich *et al.* (2005) argue that the historical sedimentation regime is due largely to natural processes. Likewise, damming of the river has trapped sediment (presumably predominantly coarse rather than fine fraction) within the basin. Such anthropogenic activities may have altered the dynamics of the fluvial system by: (i) increasing suspended load (mud) export due to enhanced soil erosion following deforestation; and/or (ii) altering bedload (sand) export due to preferential removal of sand from the river basin or destabilization of river banks through mining, or by trapping behind dams. However, none of these factors would have affected this system prior to *ca* 200 BP. By contrast, the initial shift to a mixed sand and mud regime occurred as early as 5 ka, and the gradual transition to an entirely muddy system was nearly complete by 1 ka. Nonetheless, anthropogenic activities may partially explain the sedimentology of the modern beach and foredune ridge at Tijucas, which are relatively coarse (medium to coarse sand) compared to sandy beachface deposits that predate widespread anthropogenic activity (fine to medium sand; Fig. 7).

## Autogenic basin infilling

Only a single mechanism fully explains each of the observations of changes across the Tijucas Strandplain: a gradual decrease in accommodation resulting dominantly from the trapping and deposition of fluvially derived mud in the nearshore region of Tijucas Bay (Fig. 11B to E). Maximum accommodation was available at RSL highstand, prior to the onset of progradation. The Tijucas shoreline was fronted at that time by a relatively deep bay and RSL was at its maximum, together accounting for a total water depth of *ca* 18 m at the position of the modern shoreline. Bordering steep headlands and nearby islands reduced wave energy but were also indicative of a deeply embayed shoreline: at present, the distance from the shoreline to the outer headland of 'Monkey Hill' is 12 km; it was closer to 18 km at the highstand. This allowed for the trapping and accumulation of mud in the shoreface and nearshore. Simultaneously, RSL fell *ca* 3·1 m during the period of progradation, further reducing accommodation; however, this accounts for only *ca* 17% of the loss of accommodation at the modern shoreline. As bay accommodation decreased, relative available space for mud within the bay decreased, resulting in an increase in mud deposition along the shore, and an overall increase in strandplain mud content (Fig. 11C to E).
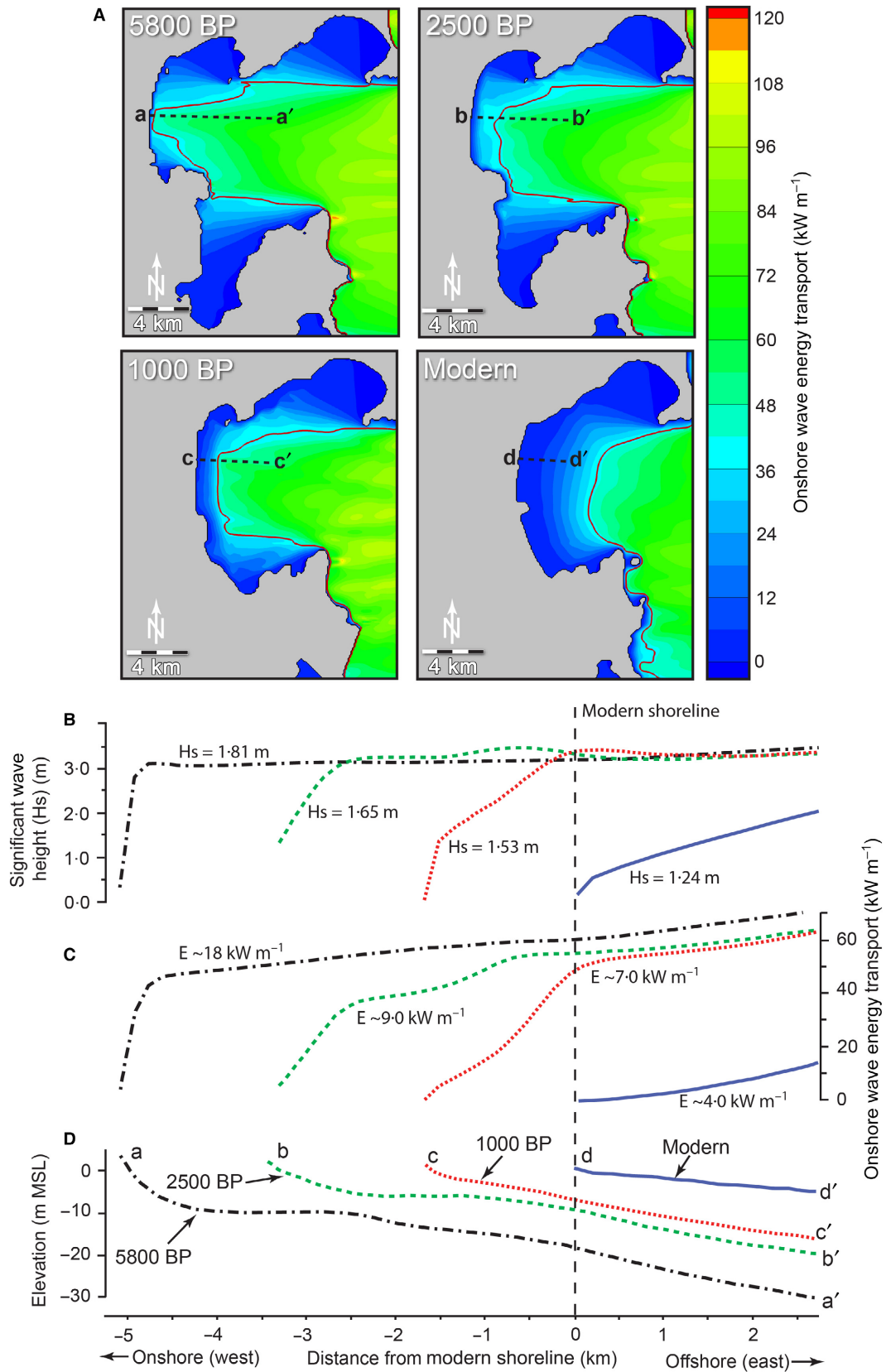
Decreased accommodation in the nearshore requires a smaller volume of sediment to fill the available space, thereby reducing the thickness of the strandplain (Fig. 6) and increasing its progradation rate (Fig. 8A). Gradual shoaling of the fronting bay through mud deposition (Fig. 9F) also increased bottom friction effects, thereby decreasing near-bed orbital velocities. Likewise, shoaling waves, particularly high during high wave-energy events, would have resuspended bottom mud, promoting turbidity and further dampening the incident wave energy. This lowered the maximum competency of the wave-driven alongshore transport, reducing the grain size of sandy sections of the plain, thus further increasing the mud content of the plain, and reducing beachface slopes (Fig. 7).

Moreover, recent (probably for several centuries) development of an active fluid mud layer in the shallow nearshore (Schettini *et al.*, 2010) has further dampened the incoming waves: gradual reduction in offshore gradient resulting from bay infilling also allows ever smaller waves to entrain the bottom muds and lessen nearshore wave energy. Thus, bay infilling serves to decrease shoreline wave energy both directly, by increasing bottom friction of incoming waves, and indirectly, by allowing those same waves to rework bottom muds into the water column, thereby attenuating the waves even further.

## CONTEXT AND IMPLICATIONS

### Muddy regressive sequences in the Holocene and geological records

Holocene and modern regressive coastal systems are found throughout the world. Prominent examples have been examined in Nayarit, Mexico (Curray & Moore, 1964; Curray *et al.*, 1969), the equatorial west coast of Africa (Anthony, 1995), Kujukuri, Japan (Tamura *et al.*, 2007), and along much of the Australian (e.g. Thom & Roy, 1985; Roy *et al.*, 1994; Woodroffe & Grime, 1999; Brooke *et al.*, 2008; Oliver *et al.*, 2015; among others) and Brazilian (e.g. Dominguez *et al.*, 1987; Lessa *et al.*, 2000; Dominguez, 2006; Dillenburg & Hesp, 2009; among others) coasts. These prograding systems are commonly domi-

nated by thick, sandy shoreface, foreshore, beachface and foredune deposits. For example, the 15 km wide Tuncurry Barrier (south-east Australia) is composed of a 5 to 20 m thick, sea-ward-thickening sequence of 'clean' sand (Thom, 1984; Roy *et al.*, 1992, 1994). Located 65 km south of Tijucas, the 8·5 km wide Pin-heria Strandplain (Fig. 1A) is similarly composed of 15 m of well-sorted, fine to very fine sand. Given its shelf source, it is unsurprising that the Pinheira plain lacks a substantial muddy infill sequence (Hein *et al.*, 2013). Approximately 200 km north of Tijucas, the 5·5 km wide, 9 to 12 m thick regressive sequence at Paranaguá (Fig. 1A) is also composed almost entirely of sand (Lessa *et al.*, 1998; Angulo *et al.*, 2009). By contrast, sand comprises only *ca* 6% of the regressive deposits at Tijucas (Units V and VI). Rather, the 4 to 8 m thick regressive strandplain lithosome is under-lain by 5 to 16 m of fluvially derived mud (Fig. 4) deposited as a basin-fill sequence at higher stages of RSL and during RSL fall.

Ancient strandplains are equally abundant in the rock record. Regressive strandplain sand-stones contain significant oil reservoirs, and notably comprise 12% of all oil resources in clastic rocks in Texas (Tyler & Ambrose, 1985). These sand bodies are important targets for petroleum exploration due to their excellent primary porosity and high permeability. In a seaward direction, these potential reservoir sandstones commonly interfinger and are under-lain by organic-rich shale source rocks. Depend-ing upon the RSL history of the region, the sequence may be capped by marine mud and/or fine-grained alluvial sediment providing a strati-graphic trap. In fact, like Tijucas, many strand-plains developed in a regime of falling RSL and it is these sedimentary complexes that serve as the best analogues for falling-stage systems tracts (Plint, 1996).

An examination of strandplain facies models (e.g. Walker & James, 1992; Roy *et al.*, 1994; Cowell *et al.*, 1995; Visher, 1999; Coe *et al.*, 2003; Tamura, 2012; Allen & Allen, 2013)

demonstrates that existing models fail to show the distinctiveness and complexity of most strandplain systems, including the irregular bounding basement surface, the diversity in stacking and juxtaposition of various near-shore, beach, dune and washover facies, and the large-scale erosional and accretionary sur-faces that characterize the internal stratification of strandplains. This study provides a high-resolution view of the internal architecture and composition of the multiple transgressive–re-gressive sequences associated with the Tijucas Strandplain and offers insight into the allo-genic and autogenic processes responsible for such architecture. In this manner, it greatly enhances current understanding of the com-plex driving mechanisms behind strandplain formation and serves as an analogue for these petroleum-bearing bodies preserved in the geo-logical record.

Holocene sediments at Tijucas are as much as 20 m thick, consisting mostly of transgressive lagoonal mud overlain by nearshore mud. This sequence is overlain by regressive-phase near-shore mud, which is separated from the under-lying mud by a thin coarse lag deposit. Portions of the strandplain are topped by 2 to 8 m thick beach and dune ridge sand. Numerous strand-plains have been identified in the rock record with similar facies associations, including the Parkman Sandstone of Wyoming (Asquith, 1970; Fraser, 1989), the Upper Cretaceous Kenilworth Member of the Blackhawk Formation in Utah (Swift *et al.*, 1987), the Point Lookout Sandstone in the San Juan Basin in New Mexico and Color-ado (Wright-Dunbar *et al.*, 1992), the Gallup Sandstone of New Mexico (McCubbin, 1972; Nummedal & Molenaar, 1995) and the Cenoma-nian Dunvegan Formation of the Alberta fore-land basin (Plint, 1996). Perhaps one of the most extensive strandplains in the ancient record is the Upper Miocene Loxton–Parilla Sands that stretch >350 km across the Murray Basin in south-eastern Australia (Miranda *et al.*, 2009). This strandplain comprises more than 600 indi-vidual ridges of late Miocene to early Pliocene

**Fig. 10.** (A) Wave conditions within the Tijucas embayment at the mid-Holocene highstand (5800 BP), 2500 BP, 1000 BP and at present, as derived from SWAN model runs using re-constructed bathymetry from each time period (see Fig. 9). Red line indicates the location of where wave transport energy is equivalent to *ca* 40 kW m$^{-1}$. (B) to (D) Representative profiles of model simulated: (B) significant wave height (Hs); (C) onshore wave-energy trans-port; and (D) bathymetry with respect to modern mean sea-level (mMSL), across the Tijucas embayment [see pro-file locations in (A) and Fig. 9]. Vertical exaggeration for bathymetric profiles is 60×. Offshore deepwater boundary conditions are the same for each simulation. Values given are for Hs and onshore wave energy transport at the shoreline.
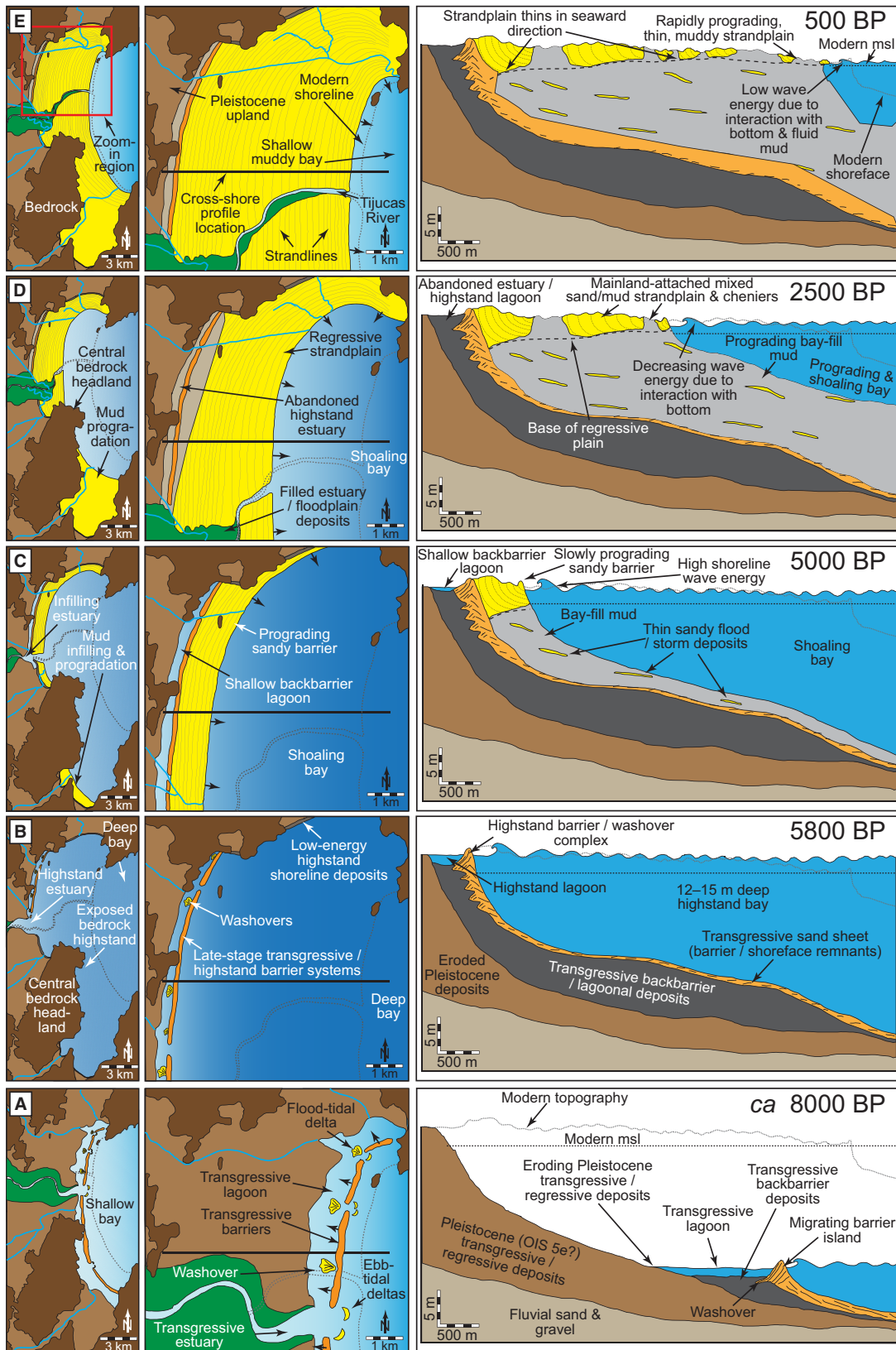
**Fig. 11.** Holocene evolution of Tijucas Bay and the Tijucas Strandplain. Simplified map and cross-section views show major events and drivers [relative sea-level (RSL) change, sedimentation and bay shoaling] of coastal change in this system from *ca* 8 ka to present.

age, which are typically 20 to 60 m thick (Roy *et al.*, 2000). In comparison, the Tijucas sandy units are generally thinner than strandplain sands reported from the rock record.

## The importance of autogenic controls on coastal evolution, sedimentary sequences and coastal response to future sea-level rise

Coastal progradation during periods of forced or normal regression is commonly characterized by the deposition of muddy and/or sandy facies. The characteristics of particular facies vary in response to trends in RSL change, rates of sediment supply, creation and filling of accommodation, and changes in hydrodynamic conditions (waves and tides) (Dalrymple *et al.*, 1992). At Tijucas, the allogenic processes of RSL fall coupled with fluvial sediment delivery and trapping within an embayment formed by fronting headlands, resulted in reduction of accommodation within Tijucas Bay. This drove autogenic feedbacks which gradually decreased wave energy, increased foreshore mud deposition, and altered the composition, beachface gradient and progradation rate of the Tijucas Beach (Fig. 11). Although allogenic processes (geological framework, RSL fall and fluvial sediment supply) are ultimately responsible for the filling of accommodation, it is autogenic feedbacks that triggered and maintained the long-term change along this shoreline. Although Tijucas probably is not unique in this sense, such feedbacks have not been heretofore recognized in Quaternary or deep-time sedimentary records.

Such autogenic feedbacks have important implications for coastal evolution. For example, prograding muddy coasts, such as found today at Tijucas, are not restricted to low-energy, embayed coasts (Fleming, 2002). Examples of moderate to high-energy muddy coasts include those of Suriname (Rine & Ginsburg, 1985), south-west India (Baba & Nayak, 2002), and the chenier plains of Louisiana (Penland & Suter, 1989) and west Africa (Anthony, 1989). These examples are commonly located in interdeltaic settings, in contrast to Tijucas which is fed directly by a river that empties into the central plain. Moreover, these coasts have been mud-dominated throughout their period of development; the Tijucas coastline had sand-dominated phases through time. By contrast, the pattern of thick muddy infill sequences underlying thin, sandy regressive shoreline deposits is generally restricted to highly embayed estuaries such as those of north-west France (Billeaud *et al.*, 2007; Tessier *et al.*, 2012), the central Northern Territory, Australia (Woodroffe *et al.*, 1993), and Benin, west Africa (Anthony *et al.*, 2002). More commonly, regressive muddy deposits are thin (for example, Bucasia, north-east Australia: Masselink & Lessa, 1995; Parangúa, Paraná, Brazil: Angulo *et al.*, 2009), or absent in strandplain sequences. Hence, stratigraphies such as that observed at Tijucas are rare, if not otherwise absent from Holocene records, a characteristic that can be attributed to its growth from sediments fed by a local mud-rich river and sequestered within a deep coastal embayment.

Another apparently distinctive aspect of Tijucas is the observed acceleration in progradation (or strandplain area growth), despite forming during a period of constant or decelerating RSL fall (Figs 2 and 8). Numerous authors have investigated the progradation rates of strandplain systems. Rates ranging from *ca* 0·2 to 2·0 m yr$^{-1}$ are common (see summaries of Roy *et al.*, 1994, Sawakuchi *et al.*, 2008, and Oliver *et al.*, 2015), although short-term rates as high as 7·8 m yr$^{-1}$ and 20 m yr$^{-1}$ (Bristow & Pucillo, 2006, and Guedes *et al.*, 2011, respectively) have been reported. At the proximal Pinheira Strandplain, mid to late-Holocene progradation rates were on the order of 1 to 2 m yr$^{-1}$ (Hein *et al.*, 2013), whereas at a classic site of Nayarit, Mexico they are as high as *ca* 3 m yr$^{-1}$ (Curray *et al.*, 1969). Despite this variability, almost all of these systems share a common characteristic: constant or decelerating progradation, the latter being driven either by high rates of sediment supply, or by progradation into a deepening basin (increasing accommodation) (e.g. Thom *et al.*, 1981; Roy *et al.*, 1994; Bristow & Pucillo, 2006). Only the coast of Wonboyn, Australia, may have experienced a unidirectional increase in the rate of progradation, but this occurred early in its evolution and was followed by 4000 years of linear growth (Roy *et al.*, 1994). At the Ilha Comprida in São Paulo state, Brazil, short-lived periods of faster progradation have been linked to local physiographic controls, and represent a temporary increase in accretion rate (Guedes *et al.*, 2011). By contrast, driven by accommodation reduction, Tijucas has both prograded (Fig. 8A) and grown in area (Table 2) at an ever increasingly faster and unidirectional rate throughout its period of development,

despite there being no overall trend of increase or reduction in volumetric deposition rates within the bay (Table 2).

An additional implication of this study is the role of substrate erodibility on future coastal responses to RSL rise. The Tijucas Strandplain is spatially highly heterogeneous: the plain gradually transitions from sand-dominated to mud-dominated in a seaward direction; it is entirely mud-dominated south of the Tijucas River; and the northern section contains alternating sandy and muddy segments (Fig. 6). Following >5000 years of fall, RSL in southern Brazil is currently rising, causing local to regional shifts towards erosion (Esteves *et al.*, 2002) and eventually large-scale transgression. Substrate geotechnical properties, such as erodibility, exert a primary control on the rate of shoreface retreat, sediment availability and resulting transgressive constructional features (Moore *et al.*, 2010; Hein *et al.*, 2014b). For example, at Tijucas, shoreface erosion during periods of transgression across sand-rich segments of the plain will liberate sandy sediments suitable for the formation and maintenance of barrier islands and transgressive dunes. However, transgression across, and erosion of, muddy segments of the plain provides no such sediment budget benefits. In this manner Tijucas serves as a prime example of why it will be critically important to recognize and consider the role of similar heterogeneous substrates composing the present-day upland deposits upon which the ongoing global transgression will proceed when predicting future coastal response to accelerated RSL rise.

## CONCLUSIONS

A combination of geophysical, sedimentological, geochronological and hydrodynamic modelling data provides insight into the autogenic processes controlling the evolution of the 75 km$^2$ Tijucas Strandplain in central Santa Catarina, Brazil. Holocene coastal deposits are underlain by a series of Pleistocene fluvial, transgressive and regressive lithosomes, the latter probably associated with the Oxygen Isotope Stage (OIS) 5e sea-level highstand. Remnants of the most recent (early to middle Holocene) transgression include a 3·5 to 8·0 m thick sequence of back-barrier lagoon deposits and thin (generally <1 m) shoreline deposits associated with a retrogradational barrier system. These transgressive deposits are preserved in their landward-most

location as a barrier-island complex consisting of a tidal channel, barrier ridge and washover deposits, backed by a 250 m wide lagoon, and dated to between 5·9 ka and 6·1 ka. Elsewhere in Tijucas the mid-Holocene highstand was marked by either an exposed bedrock coast or muddy estuarine/backbarrier deposits.

Seaward of the highstand shoreline, a 5 km wide, 6 km long and 4 to 8 m thick regressive strandplain is underlain by 5 to 16 m of seaward-thickening fluvially derived basin-fill mud. This unit creates a smoothly seaward-dipping surface onto which the strandplain accumulated as the shoreline regressed, a process initiated as a normal regression at 5·7 to 6·0 ka. South of the Tijucas River, this strandplain consists almost entirely of silt and clay. By contrast, in central and northern Tijucas, the strandplain alternates between sand-dominated and mud-dominated sections.

A gradual decrease in accommodation through time resulted dominantly (>80% at the modern shoreline) from the influx and deposition of fluvially derived mud in the nearshore, and secondarily from relative sea-level (RSL) fall. This resulted in several broad trends across the Tijucas Strandplain: (i) the sediment composition of the strandplain changes from sand-dominant proximal to the highstand shoreline to mud-dominant proximal to the modern coastline; (ii) the thickness of beachface and shoreface units that comprise the strandplain decreases from 7 to 8 m in the landward, oldest, part of the plain to <5 m proximal to the coast; and (iii) average strandplain progradation rates have increased from *ca* 0·4 m yr$^{-1}$ early in the middle Holocene to 1·8 m yr$^{-1}$ in recent centuries. Bordering headlands and islands acted to reduce wave energy and minimize export of fluvial fines to the coastal ocean. Through time, trapping of mud within the bay reduced accommodation, thus requiring a smaller volume of sediment to fill available space along the foreshore, which reduced the thickness of the strandplain and increased the shoreline progradation rate. Additionally, shoaling of the nearshore gradually reduced wave energy from 18 to 4 kW m$^{-1}$ as incoming waves interacted with the bottom further from the shoreline through time. Combined with a decrease in bay accommodation available for mud, this resulted in an increase in mud deposition along the shore and an overall increase in strandplain mud content.

The combination of allogenic (fluvial sediment supply, falling relative sea-level and geological

control) and autogenic (decreasing accommodation due to sediment trapping, wave interactions with the shoaling bay and possible shift in mud depocentre from a highstand estuary to the fronting bay) processes drove the development of a regressive system that is rare, if not unique, in the Holocene and rock records. This high-resolution study demonstrates the complexities of highstand and regressive systems tract architectures and suggests the possibility that similar systems have been un(der)-reported due to their internal complexity. Furthermore, it highlights the diverse suite of internal and external processes and feedbacks responsible for the development of an intricate assemblage of coastal sedimentary sequences.

## ACKNOWLEDGEMENTS

## REFERENCES

**Allen, P.A.** and **Allen, J.R.** (2013) *Basin Analysis: Principles and Applications*, 3rd edn. Blackwell Publishing, Oxford, 632 pp.

**Agencia Nacional da Água** (2000) Estado de Santa Catarina. Available at: hidroweb.ana.gov.br/cd3/sc.doc (accessed 18 October 2010).

**Anderson, J.**, **Milliken, K.**, **Wallace, D.**, **Rodriguez, A.** and **Simms, A.** (2010) Coastal impact underestimated from rapid sea level rise. *EOS Trans. Am. Geophys. Union*, **91**, 205–206.

**Andrade, A.C.S.**, **Dominguez, J.M.L.**, **Martin, L.** and **Bittencourt, C.S.P.** (2003) Quaternary evolution of the Caravelas strandplain, southern Bahia State, Brazil. *An. Acad. Brasil. Cienc.*, **75**, 357–382.

**Angulo, R.J.**, **Giannini, P.C.F.**, **Suguio, K.** and **Pessenda, L.C.R.** (1999) The relative sea-level changes in the last 5500 years southern Brazil (Laguna-Imbituba region, Santa Catarina State) based on vermetid $^{14}$C ages. *Mar. Geol.*, **159**, 327–339.

**Angulo, R.J.**, **Souza Filho, M.C.d.**, **Reimer, P.** and **Sasoka, S.K.** (2005) Reservoir effect of the southern and southeastern Brazilian coast. *Radiocarbon*, **47**, 67–73.

**Angulo, R.J.**, **Lessa, G.C.**, and **Filho Souza, M.C.d.** (2006) A critical review of mid- to late-Holocene sea-level fluctuations on the eastern Brazilian coastline. *Quatern. Sci. Rev.*, **25**, 486–506.

**Angulo, R.J.**, **Lessa, G.C.** and **Souza Filho, M.C.d.** (2009) The Holocene barrier systems of Paranaguá and northern Santa Catarina Coasts, southern Brazil. In: *Geology and Geomorphology of Holocene Coastal Barriers of Brazil* (Eds S. Dillenburg and P. Hesp), pp. 2–44. Springer, Berlin.

**Anthony, E.J.** (1989) Chenier plain development in northern Sierra Leone, West Africa. *Mar. Geol.*, **90**, 297–309.

**Anthony, E.J.** (1995) Beach-ridge development and sediment supply: examples from West Africa. *Mar. Geol.*, **129**, 175–186.

**Anthony, E.J.**, **Oyédé, L.M.** and **Lang, J.** (2002) Sedimentation in a fluvially infilling barrier-bound, estuary on a wave-dominated microtidal, coast: the Ouémé River estuary, Benin, West Africa. *Sedimentology*, **49**, 1095–1112.

**Araújo, A.G.M.**, **Neves, W.A.** and **Pilo, L.B.** (2003) Eventos de seca no Holoceno e suas implicaçōes no povoamento pré-histórico do Brasil Central. In: *Anais do IX Congresso da Associação Brasileira de Estudos do Quaternário (ABEQUA)*, Recife, Pernambuco.

**Ashton, A.D.** and **Giosan, L.** (2011) Wave-angle control of delta evolution. *Geophys. Res. Lett.*, **38**, L13405.

**Asp, N.E.**, **Buynevich, I.V.**, **Siegle, E.**, **FitzGerald, D.**, **Klein, A.H.F.**, **Cleary, W.C.** and **Angulo, R.J.** (2005) Coastal geomorphology of the Tijucas plain – Brazil: preliminary evolutionary model. In: Abstracts of the 10° Congresso da ABEQUA, Guarapari.

**Asquith, D.O.** (1970) Depositional topography and major marine environments, late Cretaceous, Wyoming. *Am. Assoc. Petrol. Geol. Bull.*, **54**, 1184–1224.

**Baba, M.** and **Nayak, S.** (2002) Muddy coasts of India. In: *Muddy Coasts of the World: Processes, Deposits and Function, 4* (Eds T. Healy, Y. Wang and J.-A. Healy), pp. 375–390. Elsevier Science, Amsterdam.

**Barletta, R.C.** and **Calliari, L.J.** (2001) Determinação da intensidade das tempestades que atuam no litoral do Rio Grande do Sul, Brasil. *Pesquisas Geociên.*, **28**, 117–124.

**Basei, M.A.S.**, **Campos Neto, M.C.**, **Castro, N.A.**, **Nutman, A.P.**, **Wemmer, K.**, **Yamamoto, M.T.**, **Hueck, M.**, **Osako, L.**, **Siga, O.** and **Passarelli, C.R.** (2011) Tectonic evolution of the Brusque Group, Dom Feliciano belt, Santa Catarina, Southern Brazil. *J. S. Am. Earth Sci.*, **32**, 324–350.

**Behling, H.** (1995) Investigations into the late Pleistocene and Holocene history of vegetation and climate in Santa Catarina (S Brazil). *Vegetation Hist. Archaeobotany*, **4**, 127–152.

**Behling, H.**, **Pillar, V.D.**, **Orloci, L.** and **Bauermann, S.G.** (2004) Late Quaternary Araucaria forest, grasslands (Campos), fire and climate dynamics, studied by high-resolution pollen, charcoal and multivariate analysis of the Cambará do Sul core in Southern Brazil. *Palaeogeog. Palaeoclimatol. Palaeoecol.*, **203**, 277–297.

**Belknap, D.F.** and **Kraft, J.C.** (1985) Influence of antecedent geology on stratigraphic preservation potential and

evolution of Delaware's barrier systems. *Mar. Geol.*, **63**, 235–262.

**Billeaud, I.**, **Tessier, B.**, **Lesueur, P.** and **Caline, B.** (2007) Preservation potential of highstand coastal sedimentary bodies in a macrotidal basin: Example from the Bay of Mont-Saint-Michel, France. *Sed. Geol.*, **202**, 754–775.

**Blaauw, M.** (2010) Methods and code for 'classical' age-modelling of radiocarbon sequences. *Quatern. Geochronol.*, **5**, 512–518.

**Blum, M.D.** and **Roberts, H.H.** (2009) Drowning of the Mississippi Delta due to insufficient sediment supply and global sea-level rise. *Nature Geosci.*, **2**, 488–491.

**Blum, M.D.** and **Törnqvist, T.E.** (2000) Fluvial responses to climate and sea-level change: a review and look forward. *Sedimentology*, **47**, 2–48.

**Booij, N.**, **Ris, R.C.** and **Holthuijsen, L.H.** (1999) A third-generation wave model for coastal regions, Part I, Model description and validation. *J. Geophys. Res.*, **C4**(104), 7649–7666.

**Bristow, C.S.** and **Pucillo, K.** (2006) Quantifying rates of coastal progradation from sediment volume using GPR and OSL, Holocene fill of Guichen Bay, southeast South Australia. *Sedimentology*, **53**, 769–788.

**Bronk Ramsey, C.** (2009) Bayesian analysis of radiocarbon dates. *Radiocarbon*, **51**, 337–360.

**Brooke, B.**, **Lee, R.**, **Cox, M.**, **Olley, J.** and **Pietsch, T.** (2008) Rates of shoreline progradation during the last 1700 years at Beachmere, Southeastern Queensland, Australia, based on optically stimulated luminescence dating of beach ridges. *J. Coastal Res.*, **24**, 640–648.

**Bull, W.B.** (1991) *Geomorphic Responses to Climate Change*. Oxford University Press, New York, NY, 326 pp.

**Buynevich, I.V.**, **Asp, N.E.**, **FitzGerald, D.M.**, **Cleary, W.C.**, **Klein, A.H.F.**, **Siegle, E.** and **Angulo, R.J.** (2005) Mud in the surf: nature at work in a Brazilian bay. *EOS Trans. Am. Geophys. Union*, **86**, 301.

**Buynevich, I.V.**, **FitzGerald, D.M.** and **Goble, R.J.** (2007) An increase in North Atlantic storm activity over the past 500 years: evidence from optically dated relict beach scarps. *Geology*, **35**, 543–546.

**Buynevich, I.V.**, **Klein, H.F.**, **FitzGerald, D.M.**, **Cleary, W.J.**, **Hein, C.**, **Veiga, F.**, **Angulo, R.J.**, **Asp, N.E.** and **Petermann, R.M.** (2011) Geological legacy of storm erosion along a high-energy indented coastline: northern Santa Catarina, Brazil. *J. Coastal Res.*, **SI 64**, 1840–1844.

**Caruso Jr, E.A.** (2004) Estudo de Impacto Ambiental da Atividade de Mineração de Areia, Argila e Saibro na Bacia Hidrográfica do Rio Tijucas - SC, Florianópolis, 1456 pp.

**Caruso, F., Jr**, **Suguio, K.** and **Nakamura, T.** (2000) The Quaternary geological history of the Santa Catarina southeastern region (Brazil). *An. Acad. Brasil. Cienc.*, **72**, 257–270.

**Catuneanu, O.** (2006) *Principles of Sequence Stratigraphy*. Elsevier Science, Amsterdam, 375 pp.

**Chappell, J.** (2002) Sea-level changes forced ice breakouts in the last glacial cycle: new results from coral terraces. *Quatern. Sci. Rev.*, **21**, 1229–1240.

**Church, J.A.**, **Clark, P.U.**, **Cazenave, A.**, **Gregory, J.M.**, **Jevrejeva, S.**, **Levermann, A.**, **Merrifield, M.A.**, **Milne, G.A.**, **Nerem, R.S.**, **Nunn, P.D.**, **Payne, A.J.**, **Pfeffer, W.T.**, **Stammer, D.** and **Unnikrishnan, A.S.** (2014) Sea level change. In: *Climate Change 2013: The Physical Science Basis. Contribution of Working Group I to the Fifth Assessment Report of the Intergovernmental Panel on Climate Change* (Eds T.F. Stocker, D. Qin, D.-K. Plattnerm,

M.M.B. Tignor, S.K. Allen, J. Boschung, A. Nauels, Y. Xia, V. Bex and P.M. Midgley), pp. 1137–1216. Cambridge University Press, Cambridge.

**Cleary, W.J.**, **Smith, M.S.**, **FitzGerald, D.M.**, **Doughty, S.D.**, **Silva, G.M.d.** and **Klein, A.H.d.F**. (2004) Provenance of beach sands along southern Brazilian strandplains, Santa Catarina, Brazil. *Geol. Soc. Am. Abstracts Programs*, **37**, 16.

**Coe, J.A.**, **Ellis, W.L.**, **Godt, J.W.**, **Savage, W.Z.**, **Savage, J.E.**, **Michael, J.A.**, **Kibler, J.D.**, **Powers, P.S.**, **Lidke, D.J.** and **Debray, S.** (2003) Seasonal movement of the Slumgullion landslide determined from Global Positioning System surveys and field instrumentation, July 1998-March 2002. In: *Remote Sensing and Monitoring of Landslides* (Eds J. Wasowski and V. Singhroy), *Eng. Geol.*, **68**, 67–101.

**Cowell, P.J.**, **Roy, P.S.** and **Jones, R.A.** (1995) Simulation of large-scale coastal change using a morphological behavior model. *Mar. Geol.*, **126**, 45–61.

**Cruz, F.W.**, **Vuille, M.**, **Burns, S.J.**, **Wang, X.**, **Cheng, H.**, **Werner, M.**, **Edwards, R.L.**, **Karmann, I.**, **Auler, A.S.** and **Nguyen, H.** (2007) Orbitally driven east-west antiphasing of South American precipitation. *Nature Geosci.*, **2**, 210–214.

**Cruz, F.W.**, **Burns, S.J.**, **Jercinovic, M.**, **Karmann, I.**, **Sharp, W.D.** and **Vuille, M.** (2009) Evidence of rainfall variations in Southern Brazil from trace element ratios (Mg/Ca and Sr/Ca) in a Late Pleistocene stalagmite. *Geochim. Cosmochim. Acta*, **71**, 2250–2263.

**Curray, J.R.** (1964) Transgressions and regressions. In: *Papers in Marine Geology* (Ed. R.L. Miller), pp. 175–203. MacMillan, New York, NY.

**Curray, J.R.** and **Moore, D.G.** (1964) Pleistocene deltaic progradation of continental terrace, Costa de Nayarit, Mexico. In: *Marine Geology of the Gulf of California. A Symposium Memoir* (Eds T.H. van Andel and G.G. Shore Jr), pp. 193–215. AAPG, Tulsa, OK.

**Curray, J.R.**, **Emmel, F.J.** and **Crampton, P.J.S.** (1969) Holocene history of a strand plain, lagoonal coast, Nayarit, Mexico. In: *Coastal Lagoons, A Symposium, Memoir of the International Symposium on Coastal Lagoons (Origin, Dynamics and Productivity)*, 28–30 November, 1967 (Eds C.A. Ayala and F.B. Phleger), pp. 63–100. National University of Mexico-United Nations Economic Scientific and Cultural Organizations (UNAM-UNESCO), Mexico City.

**Dalrymple, R.W.**, **Zaitlin, B.A.** and **Boyd, R.** (1992) Estuarine facies models: conceptual basis and stratigraphic implications. *J. Sed. Petrol.*, **62**, 1130–1146.

**Desastre** (2008) Enchentes 2008, Defesa Civil Santa Catarina. Available at: http://www.desastre.sc.gov.br/index.php (accessed 1 October 2010).

**Dillenburg, S.R. and Hesp, P.A.** (Eds) (2009) *Geology and Geomorphology of Holocene Coastal Barriers of Brazil*. Springer, Berlin, 380 pp.

**Dominguez, J.M.L.** (2006) The coastal zone of Brazil: an overview. *J. Coastal Res.*, **SI 39**, 16–20.

**Dominguez, J.M.L.**, **Martin, L.** and **Bittencourt, A.C.S.P**. (1987) Sea-level history and Quaternary evolution of river mouth-associated beach-ridge plains along the east-southeast Brazilian Coast: a Summary. In: *Sea-Level Fluctuation and Coastal Evolution* (Eds D. Nummedal, O.H. Pilkey and J.D. Howard), *SEPM Spec. Publ.*, **41**, 115–127.

**Dominguez, J.M.L.**, **Bittencourt, A.C.S.P.** and **Martin, L.** (1992) Controls on Quaternary coastal evolution of the east-northeastern coast of Brazil – roles of sea-level history, trade winds and climate. *Sed. Geol.*, **80**, 213–232.

Elsner, J.B., Kossin, J.P. and Jagger, T.H. (2008) The increasing intensity of the strongest tropical cyclones. *Nature*, **455**, 92–95.

Esteves, L.S., Toldo, E.E., Jr, Dillenburg, S.R. and Tomazelli, L.J. (2002) Long- and short-term coastal erosion in southern Brazil. *J. Coastal Res.*, SI 36, 273–282.

FitzGerald, D.M., Cleary, W.J., Buynevich, I.V., Hein, C.J., Klein, A.H.d.F., Asp, N.E. and Angulo, R.J. (2007) Strandplain evolution along the southern coast of Santa Catarina, Brazil. *J. Coastal Res.*, SI 50, 152–156.

FitzGerald, D.M., Hein, C.J., Cleary, W., de Menezes, J.T., Klein, A.H.d.F., Scolaro, T., Petsch, S.T. and Buynevich, I.B. (2011) Climatic and sedimentological forcing of strandplain progradation at Tijucas, Central Santa Catarina, Brazil. International Union for Quaternary Research, XVIII INQUA-Congress, 20–27 July 2011, Bern, Switzerland.

Fleming, B.W. (2002) Geographic distribution of muddy coasts. In: *Muddy Coasts of the World: Processes, Deposits and Function, 4* (Eds T. Healy, Y. Wang and J.-A. Healy), pp. 99–201. Elsevier Science, Amsterdam.

Folk, R.L. (1980) *Petrology of Sedimentary Rocks*. Hemphill Publishing Company, Austin, TX.

Fraser, G.S. (1989) *Clastic Depositional Sequences: Processes of Evolution and Principles of Interpretation*. Prentice Hall Publishing Co., Englewood Cliffs, NJ, 459 pp.

Giannini, P.C.F. (1993) Sistemas Deposicionais no Quaternário Costeiro entre Jaguaruna e Imbituba, SC. PhD Thesis. Institute of Geosciences, University of São Paulo, SP, Brasil, 439 pp.

Gouveia, S.E.M., Pessenda, L.C.R., Aravena, R., Boulet, R., Scheel-Ybert, R., Bendassoli, J.A., Ribeiro, A.S. and Freitas, H.A. (2002) Carbon isotopes in charcoal and soils in studies of paleovegetation and climate changes during the late Pleistocene and the Holocene in the southeast and centerwest regions of Brazil. *Global Planet. Change*, **33**, 95–106.

Guedes, C.C.F., Giannini, P.C.F., Sawakuchi, A.O., DeWitt, R., Nascimento, D.R., Jr, Aguiar, V.A.P. and Rossi, M.G. (2011) Determination of controls on Holocene barrier progradation through application of OSL dating: the Ilha Comprida Barrier example, Southeastern Brazil. *Mar. Geol.*, **285**, 1–16.

Hein, C.J., FitzGerald, D.M., Cleary, W.J., Albernaz, M.B., de Menezes, J.T. and Klein, A.H.F. (2013) Evidence for a transgressive barrier within a regressive strandplain system: implications for complex coastal response to environmental change. *Sedimentology*, **60**, 469–502.

Hein, C.J., FitzGerald, D.M., Buynevich, I.V., van Heteren, S. and Kelley, J.T. (2014a) Evolution of paraglacial coasts in response to changes in fluvial sediment supply. *Geol. Soc. London. Spec. Publ.*, **388**, 247–280.

Hein, C.J., FitzGerald, D.M., de Menezes, J.T., Cleary, W.J., Klein, A.H.F. and Albernaz, M.B. (2014b) Coastal response to late-stage transgression and sea-level highstand. *Geol. Soc. Am. Bull.*, **126**, 459–480.

Hein, C.J., Georgiou, I.Y., FitzGerald, D.M., de Souza, L.H.P., Klein, A.H.F. and de Menezes, J.T. (2015) Wave energy, sediment supply, and sea-level fall: Late Holocene basin infilling in southern Brazil. In: *Coastal Sediments '15, Proceedings of the 11th International Symposium on Coastal Engineering and Science of Coastal Sediment Processes*, San Diego, California.

Hesp, P., Dillenburg, S., Barboza, E.G., Tomazelli, L.J., Ayup-Zouain, R.N., Esteves, L., Gruber, N., Toldo, E.J.,

Tabajara, L. and Clerot, L.C.P. (2005) Beach ridges, foredunes or transgressive dunefields? Definitions and initiation, and an examination of the Torres to Tramandai barrier system, southern Brazil. *An. Acad. Brasil. Cienc.*, **77**, 493–508.

Hogg, A.G., Hua, Q., Blackwell, P.G., Niu, M., Buck, C.E., Guilderson, T.P., Heaton, T.J., Palmer, J.G., Reimer, P.J., Reimer, R.W., Turney, C.S.M. and Zimmerman, S.R.H. (2013) SHCal13 Southern Hemisphere calibration, 0–50,000 cal yr BP. *Radiocarbon*, **55**, 1889–1903.

Holzer, T.L. and Galloway, D.L. (2005) Impacts of land subsidence caused by withdrawal of underground fluids in the United States. In: *Humans as Geologic Agents* (Eds J. Ehlen, W.C. Haneberg and R.A. Larson), vol. XVI, pp. 87–99. Geological Society of America Reviews in Engineering Geology, Boulder, CO.

Horn Filho, N.O. and Diehl, F.L. (1994) Geologia da Planície Costeira de Santa Catarina. *Alcance*, **1**, 95–102.

Isla, F.I. (1989) Holocene sea-level fluctuation in the southern hemisphere. *Quatern. Sci. Rev.*, **8**, 359–368.

Jacques, P.D., Machado, R., Oliveira, R.G.D., Ferreira, F.J.F., Castro, L.G.D. and Nummer, A.R. (2014) Correlation of lineaments (magnetic and topographic) and Phanerozoic brittle structures with Precambrian shear zones from the basement of the Paraná Basin, Santa Catarina State, Brazil. *Braz. J. Geol.*, **44**, 39–54.

Jerolmack, D. and Paola, C. (2010) Shredding of environmental signals by sediment transport. *Geophys. Res. Lett.*, **37**, L19401.

Kirwan, M.L., Murray, A.B., Donnelly, J.P. and Corbett, D.R. (2011) Rapid wetland expansion during European settlement and its implication for marsh survival under modern sediment delivery rates. *Geology*, **39**, 507–510.

Klein, A.H.F. (1997) Regional climate. In: *Subtropical Convergence Environments: The Coast and Sea in the Southwestern Atlantic* (Eds U. Seeliger, C. Odebrecht and J.P. Castello), pp. 5–7. Springer-Verlag, Heidelberg.

Leeder, M.R., Harris, T. and Kirkby, M.J. (1998) Sediment supply and climate change: implications for basin stratigraphy. *Basin Res.*, **10**, 7–18.

Leonhardt, A. and Lorscheitter, M.L. (2010) The last 25,000 years in the Eastern Plateau of Southern Brazil according to Alpes de São Francisco record. *J. S. Am. Earth Sci.*, **29**, 454–463.

Lessa, G.C., Meyers, S.R. and Marone, E. (1998) Holocene stratigraphy in the Paranaguá Bay Estuary, southern Brazil. *J. Sed. Res.*, **68**, 1060–1076.

Lessa, G.C., Angulo, R.J., Giannini, P.C. and Araujo, A.D. (2000) Stratigraphy and Holocene evolution of a regressive barrier in south Brazil. *Mar. Geol.*, **165**, 87–108.

Lin, N., Emanuel, K., Openheimer, M. and Vanmarcke, E. (2012) Physically based assessment of hurricane surge threat under climate change. *Nat. Climate Change*, **2**, 462–467.

Marengo, J.A., Liebmann, B., Grimm, A.M., Misra, V., Silva Dias, P.L., Cavalcanti, I.F.A., Carvalho, L.M.V., Berbery, E.H., Ambrizzi, T., Vera, C.S., Saulo, A.C., Nogues-Paegle, J., Zipser, E., Seth, A. and Alves, L.M. (2012) Recent developments on the South American monsoon system. *Int. J. Climatol.*, **32**, 1–21.

Martinho, C.T., Dillenburg, S.R. and Hesp, P.A. (2008) Mid to late Holocene evolution of transgressive dunefields from Rio Grande do Sul coast, southern Brazil. *Mar. Geol.*, **256**, 49–64.

**Masselink, G.** and **Lessa, G.** (1995) Barrier stratigraphy on the macrotidal central Queensland Coastline, Australia. *J. Coastal Res.*, **11**, 454–477.

**McCubbin, D.G.** (1972) Facies and paleocurrents of gallup sandstone: model for alternating deltaic and strand-plain progradation. *AAPG Bull.*, **56**, 638.

**McTaggart-Cowan, R.**, **Bosart, L.F.**, **Davis, C.A.**, **Atallah, E.H.**, **Gyakum, J.R.** and **Emanuel, K.A.** (2006) Analysis of hurricane catarina (2004). *Mon. Weather Rev.*, **134**, 3029–3053.

**Meckel, T.A.**, **Ten Brink, U.S.** and **Williams, S.J.** (2007) Sediment compaction rates and subsidence in deltaic plains: numerical constraints and stratigraphic influences. *Basin Res.*, **19**, 19–31.

**Milliman, J.D.** and **Farnsworth, K.L.** (2011) *River Discharge to the Coastal Ocean: A Global Synthesis*. Cambridge University Press, New York, NY, 392 pp.

**Milne, G.A.**, **Long, A.J.** and **Bassett, S.E.** (2005) Modelling Holocene relative sea-level observations from the Caribbean and South America. *Quatern. Sci. Rev.*, **24**, 1183–1202.

**Milne, G.A.**, **Gehrels, W.R.**, **Hughes, C.W.** and **Tamisiea, M.E.** (2009) Identifying the causes of sea-level change. *Nature Geosci.*, **2**, 471–478.

**Miranda, J.A.**, **Wallace, M.W.** and **McLaren, S.** (2009) Tectonism and eustacy across a Late Miocene strandplain: The Loxton-Parilla Sand, Murray Basin, southeastern Australia. *Sed. Geol.*, **219**, 24–43.

**Mitrovica, J.X.** and **Milne, G.A.** (2002) On the origin of late Holocene sea-level highstands within equatorial ocean basins. *Quatern. Sci. Rev.*, **21**, 2179–2190.

**Moore, L.J.**, **List, J.H.**, **Williams, S.J.** and **Stolper, D.** (2010) Complexities in barrier island response to sea level rise: insights from numerical model experiments, North Carolina outer banks. *J. Geophys. Res.*, **115**, F03004.

**Muto, T.** and **Steel, R.J.** (2004) Autogenic response of fluvial deltas to steady sea-level fall: implications from flume-tank experiments. *Geology*, **32**, 401–404.

**Nummedal, D.** and **Molenaar, C.M.** (1995) Sequence stratigraphy of ramp setting strand plain successions: the Gallup Sandstone, New Mexico. In: *Sequence Stratigraphy of Foreland Basin Deposits, Outcrop and Subsurface Examples from the Cretaceous of North America* (Eds J.C. Van Wagner and G.T. Bertram), *AAPG Mem.*, **64**, 277–310.

**Oliver, T.S.N.**, **Dougherty, A.J.**, **Gliganic, L.A.** and **Woodruff, C.D.** (2015) Towards more robust chronologies of coastal progradation: optically stimulated luminescence ages for the coastal plain at Moruya, south-eastern Australia. *Holocene*, **25**, 536–546.

**Orselli, J.** (1986) Climatologia. In: *Atlas de Santa Catarina* (Ed. Gaplan-Gabinete de Planejamento e Coordenação Geral), vol. 2, pp. 38–39. Gabinete de Planejamento e Coordenação Geral, Rio de Janeiro, Brasil.

**Otvos, E.G.** (2000) Beach ridges – definitions and significance. *Geomorphology*, **32**, 83–108.

**Otvos, E.G.** (2005) Beach ridges. In: *Encyclopaedia of Coastal Science.* (Ed. M.L. Schwartz), pp. 172–177. Springer, New York, NY.

**Penland, S.** and **Suter, J.R.** (1989) The geomorphology of the Mississippi River Chenier Plain. *Mar. Geol.*, **90**, 231–258.

**Plint, A.G.** (1996) Marine and nonmarine systems tracts in fourth order sequences in the Early-Middle-Cenomanian, Dunvegan Alloformation, northeastern British Columbia, Canada. In: *High Resolution Sequence Stratigraphy:*

*Innovations and Applications* (Eds J. Howell and J.D. Aitken). *Geol. Soc. London. Spec. Publ.*, **104**, 159–191.

**Poland, J.F.** and **Davis, G.H.** (1969) Land subsidence due to withdrawal of fluids. In: *Reviews in Engineering Geology* (Eds D.J. Varnes and G. Kiersch), *Geol. Soc. Am. Spec. Pap.*, **2**, 187–269.

**Prado, L.F.**, **Wainer, I.**, **Chiessi, C.M.**, **Ledru, M.-P.** and **Turcq, B.** (2013) A mid-Holocene climate reconstruction for eastern South America. *Clim. Past*, **9**, 2117–2133.

**Reimer, P.J.**, **Bard, E.**, **Bayliss, A.**, **Beck, J.W.**, **Blackwell, P.G.**, **Bronk Ramsey, C.**, **Buck, C.E.**, **Cheng, H.**, **Edwards, R.L.**, **Friedrich, M.**, **Grootes, P.M.**, **Guilderson, T.P.**, **Haflidason, H.**, **Hajdas, I.**, **Hatté, C.**, **Heaton, T.J.**, **Hoffmann, D.L.**, **Hogg, A.G.**, **Hughen, K.A.**, **Kaiser, K.F.**, **Kromer, B.**, **Manning, S.W.**, **Niu, M.**, **Reimer, R.W.**, **Richards, D.A.**, **Scott, E.M.**, **Southon, J.R.**, **Staff, R.A.**, **Turney, C.S.M.** and **Plich, J.v.d.** (2013) IntCal13 and Marine13 radiocarbon age calibration curves 0-50,000 years cal BP. *Radiocarbon*, **55**, 1869–1887.

**Rine, J.M.** and **Ginsburg, R.N.** (1985) Depositional facies of a mud shoreface in Suriname, South America: a mud analogue to sandy, shallow-marine deposits. *J. Sed. Res.*, **55**, 633–652.

**Roy, P.S.**, **Zhuang, W-Y.**, **Birch, G.F.** and **Cowell, P.J.** (1992) Quaternary geology and placer mineral potential of the Forster-Tuncurry Shelf, southeast Australia. Geol. Survey of New South Wales Report #GS 1992/201, Department of Mineral Resources, NSW, 164 pp.

**Roy, P.S.**, **Cowell, P.J.**, **Ferland, M.A.** and **Thom, B.G.** (1994) Wave-dominated coasts. In: *Coastal Evolution, Late Quaternary Shoreline Morphodynamics* (Eds R.W.G. Carter and C.D. Woodroffe), pp. 121–186. Cambridge University Press, Cambridge.

**Roy, P.S.**, **Whitehouse, J.**, **Cowell, P.J.** and **Oakes, G.** (2000) Mineral sands occurences in the Murray Basin, Southeastern Australia. *Econ. Geol.*, **95**, 1107–1128.

**Sawakuchi, A.O.**, **Kalchgruber, R.**, **Giannini, P.C.F.**, **Nascimento, D.R.**, **Guedes, C.C.F.** and **Umisedo, N.K.** (2008) The development of blowouts and foredunes in the Ilha Comprida barrier (Southeastern Brazil): the influence of Late Holocene climate changes on coastal sedimentation. *Quatern. Sci. Rev.*, **27**, 2076–2086.

**Schaeffer, M.**, **Hare, W.**, **Rahmstorf, S.** and **Vermeer, M.** (2012) Long-term sea-level rise implied by 1.5°C and 2°C warming levels. *Nat. Clim. Chang.*, **2**, 867–870.

**Schettini, C.A.F.**, **Carvalho, J.L.B.** and **Jabor, P.** (1996) Comparative hydrology and suspended matter distribution of four estuaries in Santa Catarina State, southern Brazil. In: *Proceedings from the Workshop on Comparative Studies of Temperate Coast Estuaries*, 29 July–2 August 1996, Bahia Blanca, Argentina, IADO, pp. 29–32.

**Schettini, C.A.F.**, **Almeida, D.C.D.**, **Siegle, E.** and **Alencar, A.C.B.D.** (2010) A snapshot of suspended sediment and fluid mud occurrence in a mixed-energy embayment, Tijucas Bay, Brazil. *Geo-Mar. Lett.*, **30**, 47–62.

**Secretaria de Estado do Desenvolvimento Sustentável** (2013) Levantamento Aerofotogramétrico, restituição hidrográfica e MDT do Estado de Santa Catarina na escala 1:10.000. Governo do Estado de S.C.

**Seltzer, G.**, **Rodbell, D.** and **Burns, S.J.** (2000) Isotopic evidence for Late Glacial and Holocene hydrological change in tropical South America. *Geology*, **28**, 35–38.

**Siegle, E.** and **Asp, N.E.** (2007) Wave refraction and longshore transport patterns along the southern Santa Catarina coast. *Bras. J. Oceanogr.*, **55**, 109–120.

Simms, A.R. and Rodriguez, A.B. (2015) The influence of valley morphology on the rate of bayhead delta progradation. *J. Sed. Res.*, **85**, 38–44.

Swift, D.J.P., Hudelson, P.M., Brenner, R.L. and Thompson, P. (1987) Shelf construction in a foreland basin: storm beds, shelf sandbodies, and shelf-slope depositional sequences in the Upper Cretaceous Mesaverde Group, Book Cliffs, Utah. *Sedimentology*, **34**, 423–457.

Tamura, T. (2012) Beach ridges and prograded beach deposits as palaeoenvironment records. *Earth-Sci. Rev.*, **114**, 279–297.

Tamura, T., Nanayama, F., Saito, Y., Murakami, F., Nakashima, R. and Watanabe, K. (2007) Intra-shoreface erosion in response to rapid sea-level fall: depositional record of a tectonically uplifted strand plain, Pacific coast of Japan. *Sedimentology*, **54**, 1149–1162.

Tercier, P., Knight, R. and Jol, H. (2000) A comparison of the correlation structure in GPR images of deltaic and barrier-spit depositional environment. *Geophysics*, **6**, 1142–1153.

Tessier, B., Billeaud, I., Sorrel, P., Delsinne, N. and Lesueur, P. (2012) Infilling stratigraphy of macrotidal tide-dominated estuaries. Controlling mechanisms: sea-level fluctuations, bedrock morphology, sediment supply and climate changes (The examples of the Seine estuary and the Mont-Saint-Michel Bay, English Channel, NW France). *Sed. Geol.*, **279**, 62–73.

Thom, B.G. (1984) Transgressive and regressive stratigraphies of coastal sand barriers in eastern Australia. *Mar. Geol.*, **56**, 137–158.

Thom, B.G. and Roy, P.S. (1985) Relative sea levels and coastal sedimentation in southeast Australia in the Holocene. *J. Sed. Petrol.*, **55**, 257–264.

Thom, B.G., Bowman, G.M. and Roy, P.S. (1981) Late Quaternary evolution of coastal sand barriers, Port Stephens – Myall Lakes area, central New South Wales, Australia. *Quatern. Res.*, **15**, 345–364.

Thomas, M.F. (2003) Late Quaternary sediment fluxes from tropical watersheds. *Sed. Geol.*, **162**, 63–81.

Thompson, W.G. and Goldstein, S.L. (2006) A radiometric calibration of the SPECMAP timescale. *Quatern. Sci. Rev.*, **25**, 3207–3215.

Tillman, R.W. and Siemers, C.T. (1984) Siliciclastic shelf sediments. *SEPM Spec. Publ.*, **34**, 268 pp.

Tomazelli, L.J. and Dillenburg, S.R. (2007) Sedimentary facies and stratigraphy of a last interglacial coastal barrier in south Brazil. *Mar. Geol.*, **244**, 33–45.

Törnqvist, T.E., Wallace, D.J., Storms, J.E.A., Wallinga, J., van Dam, R.L., Blaauw, M., Derksen, M.S., Klerks, C.J.W., Meijneken, C. and Snijders, E.M.A. (2008) Mississippi delta subsidence primarily caused by compaction of Holocene strata. *Nature Geosci.*, **1**, 173–176.

Truccolo, E.C. (1998) Maré meteorológica e forçantes atmosféricas locais em São Francisco do Sul – SC. Florianópolis. MSc Thesis. Universidade Federal de Santa Catarina, Florianópolis, Brasil, 100 pp.

Tucker, G.E. and Singerland, R. (1997) Drainage basin responses to climate change. *Water Resources Res.*, **33**, 2031–2047.

Tyler, N. and Ambrose, W.A. (1985) Facies architecture and production characteristics of strandplain reservoirs in the Frio Formation, Texas. Bureau of Economic Geology, The University of Texas at Austin, Austin, TX, 42 pp.

Visher, G.S. (1999) *Stratigraphic Systems: Origin and Application*. Academic Press, San Diego, CA, 700 p.

Vuille, M., Burns, S.J., Taylor, B.L., Cruz, F.W., Bird, B.W., Abbott, M.B., Kanner, L.C., Cheng, H. and Novello, V.F. (2012) A review of the South American Monsoon history as recorded in stable isotopic proxies over the past two millennia. *Climate Past Discussions*, **8**, 637–668.

Walker, R.G. and James, N.P. (eds) (1992) *Facies Models: Response to Sea Level Change*. Geological Association of Canada, Waterloo, Newfoundland, Canada 409 pp.

Wiegel, R.L. (1964) *Oceanographical Engineering*. Prentice-Hall, Englewood Cliffs, NJ, 544 pp.

Woodroffe, C.D. and Grime, D. (1999) Storm impact and evolution of a mangrove-fringed chenier plain, Shoal Bay, Darwin, Australia. *Mar. Geol.*, **159**, 303–321.

Woodroffe, C.D., Mulrennan, M.E. and Chappell, J. (1993) Estuarine infill and coastal progradation, southern van Diemen Gulf, northern Australia. *Sed. Geol.*, **83**, 257–275.

Wright, V.P. and Burchette, T.P. (1996) Shallow-water carbonate environments. In: *Sedimentary Environments: Processes, Facies and Stratigraphy* (Ed. H.G. Reading), pp. 325–394. Blackwell Science Ltd, Oxford.

Wright-Dunbar, R., Zech, R.S., Crandall, G.A. and Katzman, D. (1992) Strandplain and deltaic depositional models for the Point Lookout Sandstone, San Juan Basin and Four Corners Platform, New Mexico and Colorado. In: *San Juan Basin IV* (Eds S.G. Lucas, B.S. Kues, T.E. Williamson and A.P. Hunt), pp. 199–206. New Mexico Geological Society, 43rd Annual Fall Field Conference Guidebook, New Mexico Geological Society, Socorro, NM.

Zalán, P.V. and Oliveira, J.A.B.D. (2005) Origin and structural evolution of the Cenozoic Rift System of SE Brazil. *Bol. Geosci. Petrobras*, **13**, 269–300.

Zhou, J. and Lau, K.-M. (1998) Does a monsoon climate exist over South America? *J. Climate*, **11**, 1020–1040.